Geoscience Frontiers 16 (2025) 102030

Contents lists available at ScienceDirect

Geoscience Frontiers

journal homepage: www.elsevier.com/locate/gsf

Research Paper

Detailed in-depth mapping of the world largest anorthositic complex: Magnetic anomalies, 2.5-3D modelling and emplacement constraints of the Kunene Complex (KC), SW Angola

T. Mochales [a,*], E. Merino-Martínez [b], C. Rey-Moral [b], A. Machadinho [c,d,e], J. Carvalho [c], P. Represas [c], J.L. García-Lobón [b], M.C. Feria [f], R. Martín-Banda [b], M.T. López-Bahut [b], D. Alves [c], E. Ramalho [c], J. Manuel [g], D. Cordeiro [g]

[a] Instituto Geológico y Minero de España (CN IGME-CSIC), Unidad Zaragoza, Av. de Montañana, 1005, 50059 Zaragoza, Spain
[b] Instituto Geológico y Minero de España (CN IGME-CSIC), c/ Ríos Rosas 23, 28003 Madrid, Spain
[c] Laboratório Nacional de Energia e Geologia (LNEG), Estrada da Portela, Bairro do Zambujal, 2610-999 Amadora, Portugal
[d] Geosciences Center, University of Coimbra, Rua Sílvio Lima, Pólo II, 3030-790 Coimbra, Portugal
[e] GeoBioTec, Nova School of Science and Technology, Campus da Caparica 2829-516 Caparica, Portugal
[f] Sistemas Avanzados de Tecnología, S.A (SATEC), Av. Europa, 34 A, 28023 Madrid, Spain
[g] Instituto Geologico de Angola (IGEO), Centralidade do Kilamba, Rua Nr, Luanda, Angola

ARTICLE INFO

Article history:
Received 25 July 2024
Revised 21 January 2025
Accepted 19 February 2025
Available online 24 February 2025
Handling Editor: Masaki Yoshida

Keywords:
Angola
Kunene Complex (KC)
Magnetic prospecting
2.5 modelling
3D inversion

ABSTRACT

The Kunene Complex (KC) represents a very large Mesoproterozoic igneous body, mainly composed of anorthosites and gabbroic rocks that extends from SW Angola to NW Namibia (outcropping 18,000 km^2, NE-SW trend, and ca. 350 km long and up to 50 km wide). Little is known about its structure at depth. Here, we use recently acquired aerogeophysical data to accurately determine its hidden extent and to unravel its morphology at depth. These data have been interpreted and modelled to investigate the unexposed KC boundaries, reconstructing the upper crustal structure (between 0 and 15 km depth) overlain by the thin sedimentary cover of the Kalahari Basin. The modelling reveals that the KC was emplaced in the upper crust and extends in depth up to ca. 5 km, showing a lobular geometry and following a large NE-SW to NNE-SSW linear trend, presumably inherited from older Paleoproterozoic structures. The lateral continuation of the KC to the east (between 50 and 125 km) beneath the Kalahari Cenozoic sediments suggests an overall size three times the outcropping dimension (about 53,500 km^2). This affirmation clearly reinforces the economic potential of this massif, related to the prospecting of raw materials and certain types of economic mineralization (Fe-Ti oxides, metallic sulphides or platinum group minerals). Up to 11 lobes have been isolated with dimensions ranging from 135.5 to 37.3 km in length and 81.9 to 20.7 km in width according to remanent bodies revealed by TMI mapping. A total volume of 65,184 km^3 was calculated only for the magnetically remanent bodies of the KC. A long-lasting complex contractional regime, where large strike-slip fault systems were involved, occurred in three kinematic pulses potentially related to a change of velocity or convergence angle acting on previous Paleoproterozoic inherited sutures. The coalescent magmatic pulses can be recognized by means of magnetic anomalies, age of the bodies as well as the lineations inferred in this work: (i) Emplacement of the eastern mafic bodies and granites in a stage of significant lateral extension in a transtensional context between 1500 Ma and 1420 Ma; (ii) Migration of the mantle derived magmas westwards with deformation in a complex contractional setting with shearing structures involving western KC bodies and basement from 1415 Ma to 1340 Ma; (iii) NNW-SSE extensional structures are relocated westwards, involving mantle magmas, negative flower structures and depression that led to the formation of late Mesoproterozoic basins from 1325 Ma to 1170 Ma. Additionally, we detect several first and second order structures to place the structuring of the KC in a craton-scale context in relation to the crustal structures detected in NW Namibia.

* Corresponding author.
E-mail address: t.mochales@igme.es (T. Mochales).

https://doi.org/10.1016/j.gsf.2025.102030
1674-9871/

1. Introduction

Massif-type anorthosite complexes constitute large-scale igneous intrusions, dominantly composed of plagioclase and minor mafic mineral assemblages, frequently associated with mafic and granitic suites. Such assemblage includes minor olivine, orthopyroxene or clinopyroxene and Fe-Ti oxides (Drüppel et al., 2007). Anorthosite complexes are usually found in the Proterozoic crust, whose apparent temporal constraint seems to be linked to singular tectono-thermal conditions during this period (e.g., Ashwal and Bybee, 2017). Nevertheless, the specific crustal-forming processes that led to their formation are still a matter of debate. A proposed anorogenic model for massif-type anorthosite generation would comprise partial melting of the upper mantle or crust-mantle boundary and buoyant ascent of the plagioclase fraction, promoting the ascent and emplacement of anorthosite cumulates into the crust (e.g., Duchesne et al., 1999; Dobmeier, 2006; Maier et al., 2013). As a closely related stage, the heat supplied from mantle-derived magma underplating would cause crustal anatexis, forming the granitoid magmas usually associated with anorthosite complexes (Ashwal, 1993). On the other hand, the collisional terrane stacking model would produce upper-mantle to lower-crustal underthrusting and granite-related melt generation by anatexis of lower to middle-crustal materials (Lehmann et al., 2020). Subsequent thrusting of in-depth anorthositic melt chambers, where plagioclase floats to accumulate at the top, result in diapir-shaped magma ascent channelled through lithospheric zones of weakness, favoured by a density contrast with the partially molten country rocks (Duchesne et al., 1999; Dobmeier, 2006).

Present-day boundaries and configuration of massive anorthosite bodies are the focus of research to discern the magma plumbing system from underlying mantle sources up to the crust and to assess their spatial distribution as a potential source of relevant mineralizations. The economic potential of anorthosite intrusions, especially due to their association with deposits of Fe-Ti-V, as well as with economic host deposits, including ilmenite, magnetite, chromite and platinum-group elements, has been featured in recent publications (Maier et al., 2013; Li et al., 2014; Charlier et al., 2015). In particular, the potential of the Kunene Anorthosite Complex (KC) to host Ni-Cu-rich sulphides is considered high, although it remains relatively understudied in Angola. The eventual contemporaneity of ultrabasic satellite intrusions with the KC lobe of the Zebra Mountains of Namibia (Drüppel et al., 2007) increases the interest on base metal (Ni-Cu) research.

Previous studies have reported that anorthosites have a strong magnetic susceptibility and a natural remanent magnetization (NRM) (Piper, 1974; Larson, 2015), which means that they can retain a remanent field over geologic time. High contents in hemo-ilmenite and ubiquitous magnetite in anorthosites may contribute significantly to the intensity of magnetic anomalies (Brown and McEnroe, 2008). Processing and analysis of magnetic anomalies help to obtain geometrical information on source location, size and shape of the anomaly generating bodies, structural patterns and lithological boundaries in rocks whose ferromagnetic mineral content can be evaluated by current rock magnetism analyses. The starting hypothesis here states that considerable amounts of common ilmenite ± magnetite ± apatite anorthosite assemblages (Charlier et al., 2015) can be detected by aeromagnetic methods, based on high concentrations of magnetite. If considering the Kunene Complex (KC) was created by upwelling of large mantle-derived melts with a doming effect, the paleomagnetic remanence could therefore be assumed to have been acquired during the middle stages of the doming process (Larson, 2015). Expected KC melts would range 600–820 °C (Villanova-de-Benavent et al., 2017), therefore colling below magnetite Curie Temperature would record the prevailing magnetization. The studied samples from the Kunene Complex produce significant anomalies that maintain a strong and stable natural remanent magnetization throughout geological time. Studies on the magnetic properties of the KC indicate the ubiquity of magnetite as an accessory mineral and as the main remanence bearer in single-domain particles; directional parameters indicated significant sites to yield a mean direction $D = 259°$, $I = -46°$ ($k = 7$), suggesting reversed polarity during Proterozoic times (Piper, 1974).

The U-Pb emplacement age on zircon grains of the KC and granite-related magmas has been constrained in a broad time interval between 1530 Ma and 1340 Ma (Mayer et al., 2004; Seth et al., 2005; Baxe, 2007; Drüppel et al., 2007; McCourt et al., 2013; Kröner et al., 2015; Kröner and Rojas-Agramonte, 2017; Bybee et al., 2019; Lehmann et al., 2020; Milani et al., 2022; Merino-Martínez et al., 2024) evidencing an almost continuous mantle plumbing system throughout the Mesoproterozoic.

The arduous investigation of the KC resides in the scarce representation of Mesoproterozoic belts in the Angolan Shield, whose main outcrop is represented by the KC located in the southern margin of the Angolan Craton (Ashwal and Twist, 1994). This complex extends from southwestern Angola to northwestern Namibia, cropping out 18,000 km^2. It is characterized by a large NNE-SSW striking body, intrusive into two distinct crustal materials (Merino-Martínez et al., 2022; Rey-Moral et al., 2022): An Archean to Paleoproterozoic crystalline basement (Carvalho and Alves, 1990), to the east, composed of Neoarchean gneiss-migmatite complex and Paleoproterozoic metasedimentary and igneous rocks; and a Paleoproterozoic plutonic and metasedimentary basement to the west (e.g., Seth et al., 2003; Pereira et al., 2013; Milani et al., 2022; Campeny et al., 2023). Its eastern portion is mainly covered by the Cenozoic Kalahari Basin, preventing to determine the real dimension of the KC. However, a recent geophysical work based on the gravitational field of this composite body (Rey-Moral et al., 2022) tentatively outlines the eastern extent of the Kunene Complex. In this work, we use the aeromagnetic survey carried out in the context of the PLANAGEO (National Geology Plan of Angola) Project, with the aim of suggesting the in-depth structure of the KC and proposing an accurate delineation of boundaries of individual lobes beneath the Kalahari cover. In addition, magnetic structures of the anorthosite complex and the surrounding basement have been interpreted to sort out the distinct geodynamic episodes that could have been involved in the plumbing system and the final configuration of the complex. Combined 2.5 D and 3D modelling of gravimetric and magnetic data has been used to suggest the in-depth structure of the KC intrusions, the contrasting nature of the host-crust, and the relationship between the kinematic mechanisms for the KC emplacement, lithospheric-scale boundaries and regional geodynamic context. Unified petrophysical modelling is a step forward in reducing uncertainty for geological understanding. The 4D conception is performed by considering isotopic dating, leading to devise the possible succession of events and their inclusion in the geophysical modelling.

2. Geological setting

The Kunene Complex (KC, Fig. 1) is the largest Mesoproterozoic gabbro-anorthositic massif described on Earth (42,500 km^2; Rey-Moral et al., 2022), although the exposed western segment, 350 km long and 60 km wide, only occupies a third of its actual dimension (ca. 18,000 km^2). The KC is a large composite batholith, comprising at least twelve individual coalesced plutons (Ashwal and Twist, 1994), formed of massive anorthosite, leucotroctolite and leucogabbro, variably metasomatized (e.g., Baxe, 2007;

Drüppel et al., 2007). The anorthositic suites represent mantle-derived magmas ponded at Moho depths and crystalized polybarically until emplacement at mid-crust levels, with long-live magmas (≥100 Ma; Bybee et al., 2019). The relative enrichement in MgO, Cr and Ni, as well as O, Nd and S isotope characteristics of KC suggest primary magmas maily mantle-derived basatls. The anorthositic massifs were formed by rising of feldspathic fluids, followed by troctolitic sills and successive mafic magnetism recurrently related to mantle upwellings (Maier et al, 2013). These materials are spatially and temporally associated with granitoids and (sub)volcanic equivalents (syenite, granite, granodiorite, rhyolite, mangerite, and granite porphyries), that usually crop out surrounding the KC and as narrow corridors traversing the complex (Fig. 1; Milani et al., 2022). Major and trace element geochemistry cobined with geochronology and isotopes indicates that felsic magmatism was active for at least 90 Ma, which suite was derived from mixture of Paleoproterozoic crustal component with juvenile mantle-derived material (Milani et al., 2022). The recent investigations conducted during the PLANAGEO Project (Rodrigues et al, 2021; Merino-Martínez et al., 2024) and the latest gravity survey performed in SW Angola (Rey-Moral et al., 2022) highlighted the contrasting nature of the crystalline basement surrounding the KC and the influence of pre-Mesoproterozoic inherited structures for the emplacement of the KC.

The basement to the east of the KC, delimitated as the Cassinga Zone (CZ, Fig. 2), consists of Archean to Paleoproterozoic igneous and metamorphic rocks showing structural variations from NE-SW towards NNW-SSE directions. This basement is represented by the Jamba Group (Fig. 1), a highly deformed metavolcanic and siliciclastic sequence interlayered with banded iron formations (BIFs; Korpershoek, 1970; Carvalho, 1984; Silva, 2005); and the Gneiss Migmatite and Granite Complex, composed of weakly foliated metagranites, with U-Pb protolith ages of 2621 Ma to 2568 Ma (Delhal et al, 1969; Delhal et al., 1976; Carvalho et al., 1984; Merino-Martínez et al., 2024). Eburnean granitoids, between 1982 Ma and 1971 Ma (Merino-Martínez et al., 2024) and other Paleoproterozoic metasedimentary sequences (e.g., Silva, 2005; Silva et al., 2021) are relevant in the CZ. Low gravimetric responses of CZ suggest a thick and old crust (Rey-Moral et al., 2022).

The basement to the north and west of the KC is divided in three crustal domains, named from north to south as Central Eburnean Zone (CEZ), Namibe Zone (NZ) and Epupa Zone (EZ) (Jelsma et al., 2018; Merino-Martínez and Goicoechea, 2022) (Fig. 2). The CEZ is mainly composed of Eburnean gneissic-migmatitic and granitoid rocks dated between 2038 ± 28 Ma and 1947 ± 5 Ma (Delor et al., 2006; Jelsma et al., 2011; McCourt et al., 2013; Pereira et al., 2013; Milani et al., 2022; Merino-Martínez et al., 2024). This crustal domain is separated from the CZ by a large NNE-SSW to NE-SW trending major structural weakness zone, the Quipungo Mobile Belt (QMB) described by Torquato (1977), through which the dominant NW-SE striking fabrics of the Paleoproterozoic basement are shifted towards NE-SW directions along this large-scale deformation structure (Fig. 2). The high gravity anomaly values decrease towards moderate to low values close to the Quipungo belt (Rey-Moral et al., 2022).

To the west of the KC, the NW-SE to WNW-ESE trending crystalline basement of the NZ presents the low- to medium-grade metavolcano-sedimentary sequence of the Namibe Group (Fig. 1; Escuder-Viruete et al., 2021), formerly the Schist-Quartzite-Amphibolite Complex (Carvalho and Alves, 1993), which is intruded by a large set of felsic rocks, with minor mafic and ultramafic materials of Paleoproterozoic age (i.e., 1.84 Ga to 1.74 Ga; Pereira et al., 2011; Lehmann et al., 2020; Milani et al., 2022; Campeny et al., 2023; Ferreira et al., 2024; Merino-Martínez et al., 2024).

Medium to high-grade metamorphic materials, igneous- and sedimentary-derived, showing U-Pb protolith ages from 1.86 Ga to 1.76 Ga (Pereira et al., 2013; Lehmann et al., 2020; Milani et al., 2022) are essential in the Epupa Zone (EZ) of NW Namibia. The EZ covers the southern basement of the Namibian KC (the Zebra Mountains), and is separated from the NZ by major WNW- to ENE-trending Serpa Pinto Line (SPL; Vermaak, 1981).

The southern part of the Central Eburnean Zone and the northern segment of the Namibe Zone are partially covered by an undeformed low-grade metasedimentary sequence intercalated with metavolcanic materials (Fig. 1), commonly known as the Chela Group, 1.80 Ga and 1.75 Ga old (Pereira et al., 2011; McCourt et al., 2013). In contrast, the low-grade siliciclastic sequences found on the Oncócua Plateau (Ompupa Group) and in the Iona and Cahama regions of SW Angola (Iona Group and Cahama Formation, respectively), which unconformably overlie the KC, display U-Pb depositional ages between 1.32 Ga and 1.18 Ga (Ferreira et al., 2024; Merino-Martínez et al., 2024), linked to stress relaxation episodes after the KC emplacement during Late Mesoproterozoic times. The Chela, Ompupa and Iona groups as well as the Cahama Formation. would be part of the Paleoproterozoic to Mesoproterozoic low grade metasedimentary rocks (Fig. 1).

Further crustal extension and (deep-)mantle upwelling processes characterized the late Mesoproterozoic scenario of the SW Angolan Shield (Merino-Martínez et al., 2024). Felsic, alkaline-carbonatitic and tholeiitic magmas, dated between 1.28 Ga and 1.18 Ga (Maier et al., 2013) are distributed across the Paleoproterozoic basement of NW Namibia and scarcely S of the Angolan KC (Fig. 1). On the other hand, NNW-SSE trending basic tholeiitic dikes and sills are widely represented in both SW Angola and NW Namibia, dated between 1.13 Ga and 1.07 Ga (Silva et al., 1973; Salminen et al., 2018), intruding into the metasedimentary sequences of the Oncócua Plateau (Fig. 1). During the Neoproterozoic, the crystalline basement of the NZ and the EZ were progressively deformed westwards by a complex transpressional system comprising the Pan-African Kaoko Belt (e.g., Goscombe et al., 2005), almost negligible in the Mesoproterozoic KC (Labaredas et al., 2021). The Paleo- to Mesoproterozoic basement of SW Angola and NW Namibia was partially overlain by subsequent Neoproterozoic deposits of the Damara Sequence (Fig. 1; e.g., Tegtmeyer and Kröner, 1985; Goscombe et al., 2005, 2017). From late Cretaceous times, following the opening of the South Atlantic Ocean, the SW Angolan Shield experienced significant tectonic uplift, which facilitated the sedimentation of the subsided intracontinental Kalahari Basin (Hanson, 2003; Matmon et al., 2015). There is little information on the emplacement depths of the KAC. Usually, anorthositic complexes crystallization occurs in mid-upper crust according to Bybee et al. (2019). Following Brandt et al. (2007), the emplacement depth occurred at 20 km. The thick sedimentary sequence of the Kalahari Basin covers a substantial portion of the Angolan KC, its underlying basement and nearly the entire eastern Angola.

3. Methods

In this research, new high-resolution aerogeophysical magnetic data as a whole from SW Angola are presented for the first time to the scientific community, excepting for the study of the specific Hamutenha anomaly (Morais et al., 2023). These aeromagnetic datasets were acquired during the PLANAGEO project, the National Plan of Geology of Angola, where two different geological surveys (Instituto Geológico y Minero de España, CN IGME-CSIC, Spain, Laboratório Nacional de Energia e Geologia, LNEG, Portugal), and the Spanish enterprise Impulso Industrial Alternativo, were involved,

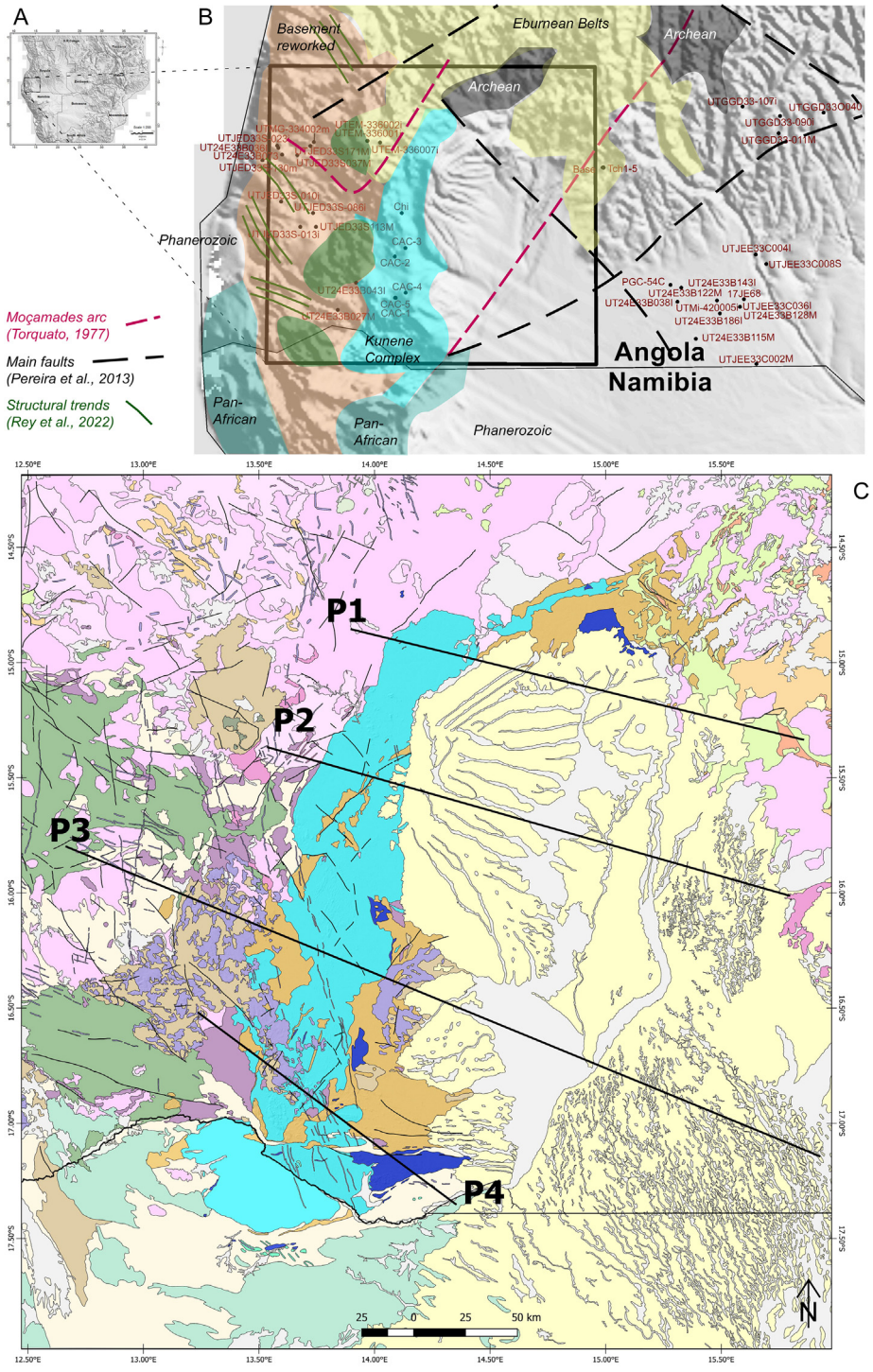

Legend

Mesozoic to Cenozoic deposits
- Quaternary sediments. Pleistocene-Holocene
- Kalahari Group. Oligocene-Pleistocene
- Meso-Cenozoic sedimentary deposits and volcanics

Archean to Neoproterozoic metamorphic basement
- Undifferentiated Neoproterozoic metasedimentary rocks
- Palaeoproterozoic to Mesoproterozoic low-grade metasedimentary rocks
- Epupa metamorphic Complex
- Palaeoproterozoic low- to high-grade metasediments (Namibe Group)
- Undifferentiated metamorphic Eburnean basement
- Palaeoproterozoic (Orosirian) undifferentiated metasediments
- Jamba Group (Neorchean)
- Neoarchean Gneiss-Migmatite Complex

Igneous Rocks
- Mesozoic alkaline-carbonatitic to tholeiitic igneous rocks
- Late-Mesoproterozoic alkaline and carbonatitic dykes
- Late-Mesoproterozoic basic subvolcanic rocks
- Mesoproterozoic basic magmatism related to the KC
- Mesoproterozoic felsic magmatism related to the KC ("Red Granites")
- Mesoproterozoic KC Anorthosites
- Early-Mesoproterozoic basic subvolcanic rocks
- Palaeoproterozoic volcanic and subvolcanics
- Palaeoproterozoic felsic igneous rocks
- Palaeoproterozoic basic igneous rocks

Fault

in collaboration with the Geological Survey of Angola (IGEO). The company Xcalibur Multiphysics was subcontracted as the geophysical operator. We use the obtained magnetic data to define magnetic anomalies (Fig. 2), structural lineaments (Fig. 3) and the in-depth configuration of the Mesoproterozoic Kunene Complex (KC), related rocks and the surrounding basement, in comparison with the gravity response of the area (Rey-Moral et al., 2022) and put it in context of a large geochronological dataset available for the KC and related rocks (i.e., Carvalho et al., 2000; Mayer et al., 2004; Seth et al., 2005; Baxe, 2007; Drüppel et al., 2007; Maier et al., 2013; McCourt et al., 2013; Kröner et al., 2015; Brower, 2017; Kröner and Rojas-Agramonte, 2017; Simón et al., 2017; Bybee et al., 2019; Lehmann et al., 2020; Milani et al., 2022) and the new U-Pb dating obtained during the PLANAGEO project (Merino-Martínez et al., 2024) to constrain the geological evolution of the KC during Mesoproterozoic times.

3.1. Dataset

(1) Magnetic data. Airborne magnetic surveys were performed between June 2014 and January 2017 to produce a national magnetic dataset. Technical specifications consisted of a nominal line spacing of 1 km, 10 km between tie lines, 100 m of terrain clearance and flight directions perpendicular to the regional geological strike. The dataset presented in this work represents about 120,000 km of flight line with a G-8223A airborne cesium magnetometer. Diurnal variations were monitored by GSM-19 base station magnetometers. The resulting map offers a complete image of the Total Magnetic Intensity Field (TMI, Fig. 2) of the study area, from which subsequent processing was performed via fast Fourier transformation (FFT), i.e., reduction to the pole (RTP), vertical and horizontal gradients and analytic signal. As the processed data and measurements of the involved units indicate that most of the magnetization is due to remanent sources, both in the mapping of magnetic units and 2.5D/3D modelling, we declined using RTP and opted for the Total Magnetic Intensity to characterize the KC intrusive complex (Fig. 2).

(2) Gravimetric data. The Bouguer anomaly data used in the 2D models of this study derive from the Bureau Gravimetrique International database (BGI, https://bgi.omp.obs-mip.fr/data-products/Gravity-Databases/Land-Gravity-data) (Balmino et al., 2012; Bonvalot et al., 2012). The Bouguer anomaly provided by the BGI is gridded 3500 m × 3500 m, which anomalies are explained by large-scale structural variations in the upper and lower crust.

(3) Petrophysical data. Analyses of rock samples have been conducted to assess if the rocks under study have a sufficiently high contrast to produce measurable magnetic and gravimetric anomalies. Thus, unified modelling has been performed, in which a simultaneous magnetic and gravimetric adjustment has been achieved, by introducing real data of magnetic susceptibility, remanence and density of the lithostratigraphic units involved. 44 representative rock samples were collected from key outcrops, from which 240 specimens were analyzed for petrophysical properties (Fig. 1; Supplementary Data Table 1). A regular sampling of the main lithological units studied was pursued, considering land inaccessibility, weathering and sedimentary covering. Densities were measured by sample water displacement and weight method with two repetitions of the measurements (variation of one hundredth of a gram). We also used previous data (Rey-Moral et al., 2022; and references therein). Magnetic susceptibility (k) analyses were carried out at room temperature on specimens of known volume with a susceptibility bridge, KLY-3S Kappabridge (AGICO) at the University of Zaragoza (Geotransfer Research Group). Natural Remanent Magnetization (NRM) of rock samples was measured in order to determine the Koenigsberger ratio (Q). A large Q (Q > 1) indicates that the magnetic material will tend to maintain a significant remanent magnetization related to small mineral grain size and therefore NRM must be incorporated into the modelling for correct interpretation (see Supplementary Data Table 1). The gravimetric/magnetic 2.5D models show the values of density, magnetic susceptibility, natural remanent magnetization and Q-ratio (Supplementary Data Table 2). Particularly relevant are the samples with low/intermediate susceptibility and high remanence.

Eleven detailed Isothermal Remanent Magnetization (IRM) acquisition curves were obtained with the aim to unravelling the magnetic mineralogy of the rocks involved. The method used to analyze the IRM curves relies on the cumulative log Gaussian method (Robertson and France, 1994), which is based on fitting the IRM acquisition curve versus the logarithm of the applied field (Fig. 4). In this case, the IRM curves were acquired in 27 steps with increasing applied field from 3 to 17 mT at low coercivity and from 20 to 250 mT at high coercivity, by means of M2T-1 Pulse Magnetizer (Ferronato) and measured by a Superconducting 755 (2G) Magnetometer (Paleomagnetism Laboratory of University of Burgos). The method discriminates the mineral components according to their coercivities that make up the IRM curve. We use a web application for unmixing magnetic coercivity distributions: MAX UnMix (Maxbauer et al, 2016; https://shinyapps.its.carleton.edu/-max-unmix/). This application allows obtaining the mean coercivity of the magnetic component, its dispersion parameter, the relative proportion of each component, and the skewness factor. Logarithmic coercivity values of ~ 1.64 mT, ~2.3 mT and ~ 3.3 mT are related to magnetite, hematite and goethite contribution, respectively.

3.2. 2.5D modelling

In this study, geological mapping and petrophysical data are first-order constraints to 2.5D modelling (Supplementary Data Table 2), whereas structural patterns extracted from field observations, derivatives and Euler depths have also been used to understand the deep configuration of the igneous bodies beneath the Cenozoic Kalahari cover. Gravity and magnetic fields are modelled together to deal with the non-unicity problem, by modifying geometry of bodies and petrophysics parameters simultaneously to fix realistic values, vertical contacts and depth layers. The profile data have been extracted from TMI and Bouguer anomaly grids with a spatial density of one data point per 0.2 km. By inputing our petrophysical data into the modelling workflow, we are able to minimize the error between the observed and calculated response, and thereby refine the optimal fit between the outcropping/subsurface units and the model. The feedback procedure ends

Fig. 1. (A) Inset of the study area in the Angola-Namibia border. (B) Detail with Phanerozoic terrains (bright grey), Archean Cratons (dark grey), Eburnean Belts 2.0–1.8 Ga (yellow), Basement reworked 1.8 Ga ago (orange), Paleo to Neoproterozoic metasedimentary rocks (Chela and Damara Groups), Kunene Complex 1.43–1.37 Ga (bright blue) with the main trends represented. The samples collected for this work are also labelled and located in red. The area is framed. (C) Geological map of SW Angola (modified from Merino-Martínez et al., 2024) and NW Namibia (synthetized from Kröner et al., 2015) with the main geological units involved in the Archean and Paleoproterozoic basement as well as the magmatic units involved in the KC. See location for the modelled sections. (For interpretation of the references to colour in this figure legend, the reader is referred to the web version of this article.)

when a reasonable congruence with the constrained depth and geometry of sources is found.

In this work, we focus on the interpretation of geophysical and geological features to understand the deep geometry and emplacement model of the KC in the Congo Craton during the Mesoproterozoic. The identified paleomagnetic pole of 1.38 Ga in the Kunene Anorthosite Complex of Angola/Namibia reported a negative polarity (declination 264° and inclination – 65°; Piper, 1974) which corresponds with antipodal orientations in normal polarity (declination 84° and dip 65°). Pre- or *syn*-fold remanence has been detected in the Zebra Mountains (Larson, 2015), supported by positive folding and conglomerate tests, proving that the unit was not remagnetized and allowing magnetic orientations to be inferred in paleogeographic terms. The magnetic components detected were mainly magnetite (decreasing in intensity at 500–580 °C) and hematite (persisting in intensity at 670 °C). The white anorthosites vary up to 1 A/m while the dark anorthosites reach magnetic moments up to 10 A/m (Larson, 2015). This context serves to support the fact that the remanence is negative, and it has not been remagnetized by subsequent events. This is the first premise to interpret that the magnetization is due to the KC and to be able to model the different units of KC based on their petrophysical particularities. In the case of the gravity modelling, the upper crust has been differentiated in three crustal portions. The dense, thin and recent upper crust is located to the W due to the opening of the South Atlantic Ocean, which oceanic crust would substitute in Cretaceous times the old, thick and relatively light Proterozoic crust. A density contrast up to $\Delta\rho$ = 100 kg/m^3 is differentiated in the Namibe-Lubango (to the NW of the study area), transitional crust and Cassinga crust (to the E) and Epupa crust (to the S).

3.3. 3D modelling

The 3D magnetic modelling was performed using the Voxi Earth Modelling extension of the Oasis montaj® software (Seequent) that performs a 3D voxel-based inversion and obtains the magnetic susceptibility distribution for the area considered in the inversion. The magnetic susceptibility model can be determined by conventional magnetic inversion (CMI) or by magnetic vector inversion (MVI). While the CMI assumes that the magnetic response arises entirely from magnetic induction, the MVI considers the presence of induced and remanent magnetization. The MVI provides a more accurate and realistic geological model, particularly if remanent magnetization is suspected or working at low latitudes (Ellis et al., 2012) as is the case of the KC.

The MVI model results include three outputs that are useful for the interpretation of magnetic anomalies: the amplitude of the magnetization and the Earth-field projection of the magnetization and the amplitude of the perpendicular-to-Earth-field component of the magnetization, where amplitudes are normalized by the strength of the inducing field. The amplitude of magnetization is the most significant scalar and should be the primary quantity used in interpretations (Ellis et al., 2012).

The scalar property returned by the MVI inversion is named the MVI susceptibility. These values can be used directly in the interpretation and can be compared and constrained by the known measured rock susceptibility when available (MacLeod and Ellis, 2013), or by the conventional data otherwise. We applied two iterations of iterative reweighting inversion (IRI) to improve the MVI inversion results and the geometry of the results and the amplitudes of the recovered physical properties (Geosoft, 2013). For each lobe model from the voxel we created several isosurfaces, representing different MVI susceptibility values (in S.I.). The distinct Mesoproterozoic rocks forming the KC, specifically anorthosites, mafic rocks (gabbros) and felsic rocks (Red granites) are characterized by intervals of MVI susceptibility values. MVI susceptibility sections were extracted from the 3D voxel models located along the 2.5D profiles (Fig. 7).

4. Results

4.1. Petrophysics

Data for middle-lower crust and Neoarchean basement have been obtained from the literature, using values of 0.001 S.I. and non-remanence under the Curie isotherm (Nafe and Drake, 1957; Lowrie, 1997). Densities have been reproduced by applying values reported in Rey-Moral et al. (2022), which are 2800 kg/m^3 for the middle-lower crust and progressively lighter upper crust according to the expected transition from the oceanic to continental crust to the thick craton: 2695 kg/m^3 for the Epupa and Namibe-Lubango basement; 2685 kg/m^3 for the transitional crust; and 2675 kg/m^3 for the Cassinga basement (further explanations in section 4.2.).

Specific samples of the Jamba Group (Supplementary Data Table 2), Neoarchean in age, yield medium susceptibility values (0.0038 S.I.), high remanence (3.8610 A/m) and density (3125 kg/m^3). The metasedimentary rocks of the Namibe Group present low magnetic susceptibility, remanence and density values (0.0002 S.I. and 0.0016 A/m, 2605 kg/m^3, respectively), showing high values in the amphibolitic terms (0.0009 S.I. and 0.0115 A/m, 2958 kg/m^3, respectively). The igneous derived samples of the Epupa metamorphic complex (orthogneisses) have high magnetic susceptibility (0.01445 S.I.), remanence (6.6806 A/m) and low density values (2623 kg/m^3). The widespread Orosirian to Statherian (i.e., Eburnean to Epupa) rocks present low and medium–high magnetic susceptibility (0.0061 S.I. for the felsic and 0.0149 S.I. for the mafic terms) with low remanence values (0.4449 A/m and 0.2084 A/m, respectively). The density is high in the felsic rocks (2767 kg/m^3), being more pronounced in the mafic terms (3054 kg/m^3). Finally, the metavolcanic materials of the Chela Group (comprised in the Paleoproterozoic to Mesoproterozoic low-grade metasedimentary rocks, Fig. 1) show low magnetic susceptibility (0.0001 S.I.), remanence (0.0403 A/m) and high density (2749 kg/m^3).

Regarding the Mesoproterozoic units related to the KC, laboratory measurements establish a marked contrast of properties between the distinct KC members and allow us to implement the petrophysical information in the modelling (Supplementary Data Table 2; see sections 4.4 and 4.5). The KC anorthosites present medium values of susceptibility (0.0040 S.I.) with high remanence (7.6518 A/m), whereas density is relatively higher than its background (2749 kg/m^3). Mafic rocks of the KC (mainly gabbros) reveal medium–high magnetic susceptibility (0.0150 S.I.), very high remanence (29.3330 A/m) and density (2810 kg/m^3). On the other hand, the felsic rocks associated with the KC (locally known as Red granites) present high values of magnetic susceptibility (0.0272 S.I.), very low remanence (0.0999 A/m) and density (2644 kg/m^3).

The Q index (Supplementary Data Table 1, Fig. 4A) reported relevant values in most of the rock types analyzed. Most lithostratigraphic units of the Jamba Group present Q index close to 1 (except for quartzites). The Orosirian sample corresponds to a migmatitic enclave with high Q index (Q = 7). The Namibe Group, amphibolite or paragneiss, presents Q values close to 1. The highest Q detected in the Namibe Group (sample 16JE187) could be thermally affected by the proximity of the KC intrusive bodies. The Paleoproterozoic felsic rocks present generally low values (Q < 1), except for the samples UT24E33B143I and UTGGD33-107i, granites belonging to the eastern basement, whose primary magnetization presents high values of remanence with regard to their susceptibilities. In the case of the granite UTJED33S-086i and gra-

nodiorite UTJED33S-013i, primary remanence or proximity to the KC intrusion may have thermally affected the sample. The analyzed Paleoproterozoic felsic rocks present low values (Q < 1). The leucogneiss and orthogneiss of the Epupa Complex present very high Q, probably related with their primary magnetization. The basalt and rhyolites of Humpata Formation (Chela Group), within the Paleo-Mesoproterozoic metasedimentary rocks, present high Q values, as expected for volcanic rocks, whereas the *meta*-sandstone (Cahama Formation, sample UTJEE33C008S) presents high Q likely due to contained volcaniclastics from denudation of the KC. The KC samples collected in this work were highlighted in the Fig. 4A. Red granites associated to KC present low Q values and high susceptibilities. On the other hand, anorthosite and gabbro of the KC present moderate magnetic susceptibilities and very high remanences, what provide very high Q values (Q > 10 and even Q ≫ 100). This marked contrast between the units from the KC serves as a starting premise for the modelling of this work.

IRM acquisition curves (Fig. 4B) denoted changes in magnetic mineralogy according to their petrogenetic origin. IRM modelling displays the mineral components of each sample related to mineral coercivities and magnetic saturation (Fig. 4, Table 1). The skewness in the modelling and the preponderance of a low coercive component (log 1.51 to 1.64 mT) would be probably related to the variable concentration and oxidation degree of magnetite. Basic rocks bear a variable proportion of ferromagnetic minerals depending on their degree of alteration. KC gabbros (CAC4A, Fig. 4) show a predominance of low coercive minerals, whereas the altered troctolite/anorthosite (CAC5A, Fig. 4) presents almost equivalent content in low and high coercive minerals (see Table 1 for percentages). On the other hand, Red granites associated to the KC have mostly high coercive minerals. Epupa felsic Paleoproterozoic rocks from the surrounding basement of the KC show up to four ferromagnetic components in the felsic fraction with majority of magnetite and minor iron sulphides, haematite and goethite for granodiorites and granites (Fig. 4, Table 1). Conversely, the Paleoproterozic mafic rocks present two clear ferromagnetic components, prevailing magnetite, against a high coercive fraction, probably goethite. Regarding the rhyolites of the Paleoproterozoic Chela Group only high coercive minerals are detected. In the Paleoproterozoic metasediments of the Namibe Group two main mineral components have been differentiated: mainly magnetite and high coercive minerals to a lesser extent (goethite or hematite).

4.2. Magnetic map and relevant sources depth of the Kunene Complex, surrounding basement and Kalahari cover thickness

The study area presents a variation of total magnetic field values characterized by significant anomalies that range from > 6,500 nT to < − 10,000 nT (Fig. 2). In general, positive anomalies (0 to 6,500 nT) are preferably distributed in the eastern quadrant of the study area, extending ~ 270 km long and 80 km wide, in NE-SW orientation. Such anomalies are interpreted to be formed by the interference of: (i) shallow notably strongly magnetized rocks, the first 20 km surrounding the main remanent bodies (negative anomalies); (ii) low positive anomalies constituting the magnetic background of the eastern study area. Other maxima magnetic anomalies are recorded on the edge of negative anomalies, spanning 10–20 km wide and 35–70 km long peaks in magnetic field intensity. These peaks would represent analogous magnetic signal of the intense shallow rocks of the eastern quadrant. The strong positive anomalies (300 nT to 7,000 nT) surrounding and separating the large negative anomalies have been attributed to the Red granites (KC_rg, Fig. 2) according to their outcropping and characteristic magnetic signal. As mentioned in section 4.1, Red granites present high susceptibility values with low remanence, which leads to registering intense magnetic signatures with positive orientation. Nevertheless, we attribute the mild intensity positive anomalies detected in the eastern quadrant to Paleoproterozoic crust. According to the affinity of the magmas of the KC, anorthosites and gabbros would correspond to mafic and ultramafic magmas, which in turn would constitute the dense and strongly remanent bodies, mainly the gabbros.

Intermediate extensive anomalies are located westwards (0 to −250 nT, with ~ 180 km in length and ~ 140 in width), and constitute the magnetic background of the area. Such magnetic signatures are interpreted as Paleoproterozoic crust. In this crust, the different Paleoproterozoic felsic rocks (Fig. 1) would have a generalized paramagnetic contribution and would be little notable on the aeromagnetic map. On the other hand, the mafic rocks (Paleoproterozoic volcanics and plutonic mafic rocks, Fig. 1) produce relative maxima randomly distributed in the NW quadrant, in various sub-annular structures. Striking negative anomalies represent the KC lobes associated to intensely remanent magnetization (opposite direction of the current magnetic field). Rock magnetic analyses (section 4.1) evidence medium–high magnetic susceptibility and very high remanence, likely acquired at the time of the consolidation of the mafic members of the KC. KC emplaced in the regions of Oncócua and Cahama, in north Angola and its southern prolongation to Namibia, to the Zebra Mountains. Six bodies have been characterized (Figs. 2 and 6) whose names correspond to their geographic localities. Chiange, Pocolo and Otchinjau lobes mostly crop out, whereas Oncócua, Chibemba W and Uanguembela do it partially. The Mutumieque basalts narrowly crop out on the Oncócua plateau (Figs. 1 and 2) and would correspond with the end of the KC intrusion. Four new lobes with outstanding dimensions, unknown so far, have been precisely outlined by means of this work: Cuvelai, Chibemba E, Queulo and Cahama lobes, located eastwards under the Kalahari sedimentary cover. Further west, thanks to this work, the Oncócua Lobe has been precisely delineated. Their dimensions have been calculated considering an ellip-

Table 1
Proportion of magnetic minerals obtained in the samples through Isothermal Remanent Magnetization cumulative log curve analysis. The curves obtained in Fig. 4 are based on the coercitity of magnetite, hematite, goethite, iron sulphides and other intermediate species probably coming from the oxidation of the magnetic material.

Unit	Lithology	Sample	%Magnetite	%Hematite	%Goethite	%Iron sulphides	%Other
KC_gb	Gabbro	CAC4a	91.5	6.4	1.6?		
KC_an	Altered troctolite/anorthosite	CAC5a	48	41	11		
KC_rg	Red grainite	17JE07-1A	11	78	11		
Pf	Granodiorite	PGC150A	63	12.4	2.1	22.5	
Pf	Granite	UTJED33S-130 *m*	49.5	11.4	31.5	4.9?	2.7 (1.9 log)
Pb	Quartzdiorite	UTJED33S-010i	95.5		4.6		
Pb	Diorite	PGC69A	90.5		9.5		
Emb	Ryolite Chela Gp	UTEM-336001i	91.9		5.8		2.3 (2.1 log)
Gnm	Paragneiss Namibe Gp	16JE187	91.8	0.7	7.5		
Gnm	Paragneiss Namibe Gp	16JE92	91.7		8.3		
Gnm	Amphibolite Namibe Gp	PGC88u-1A	90.5		9.5		

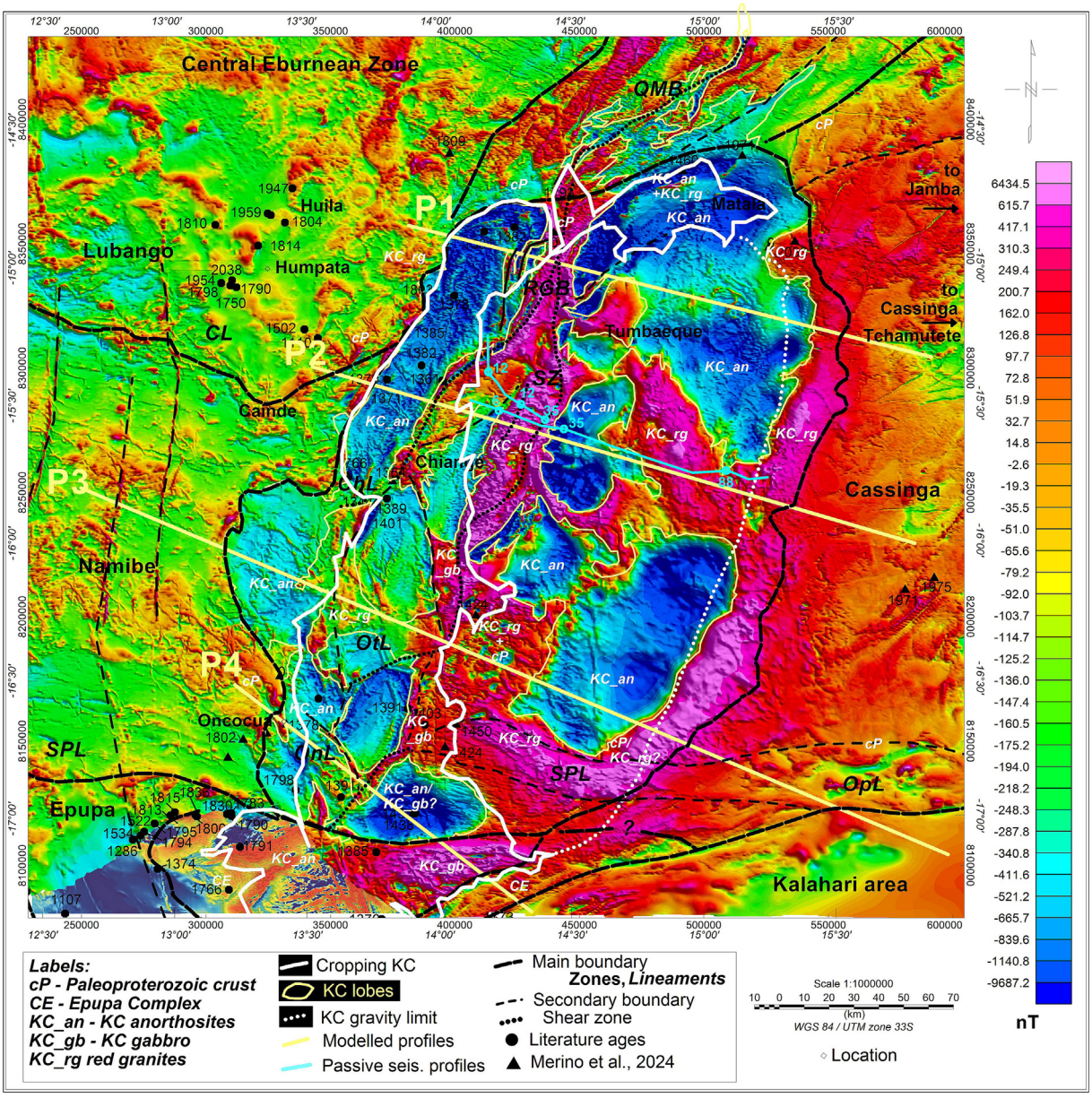

Fig. 2. TMI map of the Kunene Complex. Labels of the units detected by aeromagnetic prospection. Structural domains defined by main lineaments. Main lineaments: QMB, Quipungo Mobile Belt; RGB, Red Granite Belt; SZ, Shear Zone; ChL, Chiange Lineament; OtL, Otchinjau lineament; OnL, Oncócua Lineament; SPL, Serpa Pinto Line; OpL, Opuwo lineament. KC remanent bodies are differentiated in thin yellow line. KC outcropping is highlighted in white line. Dotted white line represents the previous gravity KC boundary (Rey-Moral et al., 2022). Modelled profiles are plotted (thick yellow line) and Passive Seismic lines (blue lines) with the depth of the lobes modelled under the Cenozoic Kalahari cover. (For interpretation of the references to colour in this figure legend, the reader is referred to the web version of this article.)

soid volume where *X* and *Y* have been measured in the TMI map and depth extracted from 2.5D modelling. Resulting volumes range from ~ 1,400 km^3 for the shallowest Pocolo Lobe to ~ 23,700 km^3 for the Cuvelai Lobe, the most extensive one (Fig. 2, Table 2). Maier et al. (2013) presented a N-S stratigraphic profile through the Zebra Mountains Lobe that encompasses a ~ 16-km-thick dome-like mass, whose lateral dimensions are ~ 80 km × 50 km. The domed sequence would fold to an undescribed depth. Assuming the average depth of the southern lobes studied in this work (4.4 km) the ellipsoidal volume for the Zebra Mountains Lobe would reach ~ 9,215 km^3. All eleven lobes sum up to ~ 65,185 km^3, just considering the remanent part of the KC (Fig. 2). If all the lobes are included with the closest part of the halo of Red granites, considering the minimum depth of 3 km (Rey-Moral et al., 2022) a volume of 134,500 km^3 results.

The KC lobes are laccolitic bodies with a strong remanent magnetization, reverse to the current magnetic field with mean orientation of Declination 259° and Inclination – 49° (Piper, 1974). This is evidenced by the highlighted negative anomalies recorded on the TMI map, with intensities up to – 10,000 nT (Fig. 2). Petrophysical analyses (section 4.1) indicate the presence of ubiquitous magnetite as accessory mineral in the gabbroid and anorthositic rocks, variably oxidized with regard to the degree of alteration. Magnetite would be the main remanence carrier, either as discrete grains and fine rods in feldspar, both in single domain magnetite (Piper, 1974), what would lead to such high remanence values, reaching 5 A/m (Piper, 1974). In this work, natural remanent magnetization shows a varied range of values (0.1–37 A/m, Supplementary Data Table 1). Medium-high susceptibility values are reported in Piper (1974) (0.012–0.75 S.I.), as values determined in this work

Table 2
Dimensions of the early Eastern lobes: Cuvelai, Chibemba E, Chibemba W, Queulo, Cahama and Chabicua and the late western lobes: Chiange, Pocolo, Otchinjau, Oncócua. Volume calculated from the ellipsoid which extension comes from the imagery and depth is obtained from modelling. The Zebra Lobe dimensions are calculated from the literature data of Maier et al. (2013). Note the non-elongated shape of the eastern lobes with regard to the western ones. This is in accordance with their first stage extensional setting, opposite to transpressive structures would be linked to the second stage of emplacement.

	Lobe	Lenght (km)	Width (km)	Depth (km)	Volume elipsoid (km^3)	
East 1.5–1.4 Ga lobes	Cuvelai	112.8	81.9	4.9	23702.15	
	Chibemba-E	59.2	26.2	5.2	4223.04	
	Chibemba-W	70.7	20.7	2.5	1921.12	
	Queulo	37.3	28.4	3	1663.98	
	Cahama	98.1	40.8	3.9	8173.21	
	Chabicua	52.8	24.7	5.1	3482.57	
West 1.4–1.3 Ga lobes	Chiange	135.5	24.8	3.6	6334.2	
	Pocolo	50.8	29.2	1.8	1398.03	
	Otchinjau	60.9	25.3	3.3	2662.26	
	Oncocua	69.9	18.8	3.5	2408.25	
	Zebra	80	50	4.4	9215.34	Maier et al., 2013
				SUM	65184.15	

(0.001–0.70 S.I.). On the other hand, the strong positive anomalies detected in the halo of the remanent lobes are due to the peripheral consolidation of Red granites, whose range of susceptibility is in mean higher than those of the mafic rocks of the KC (0.0272 S.I.), with very low remanence (0.0999 A/m).

In covered areas, either attenuation of magnetic anomalies, or change in their wavelength, hardly occur. These suggest that the source is shallow, indicating a sedimentary Kalahari thickness of tens of meters. In this sense, Kalahari cover was determined by means of an isopach map from borehole data processing (Haddon, 2005). Thickness range from 2 to 16 m in the western boundary of the KC with the Kalahari Formation. As one moves to the SE into the basin, the thickness reach up to 95 m of thickness. Additionally, two passive seismic profiles were performed in the frame of the PLANAGEO project with the goal of estimating the Kalahari cover thickness (Carvalho et al., 2024) (Fig. 2). A passive seismic profile runs from the eastern boundary of the Chiange Lobe eastwards, to the south of the Tumbaeque location (Fig. 2). The Kalahari thickness was determined as a minimum depth of 1 m in the boundary of KC with the Kalahari Formation, whereas maximum depths of the basin reached up to 200 m depth. In the southern profile, thickness departs from 1 m deep at the boundary, to ~ 50 m as first depocentre at 20 km of the profile. Subsequently the profile crosses a shallow area of 35 m at 30 km (blue circles in Fig. 2), followed by a second depocentre of 180 m deep at 60 km. From there, the shallowing of the Kalahari Basin to 88 m takes place at the 100 km of the profile (blue circles in Fig. 2). From there to the end of the profile (125 km) the basin deepens up to 200 m. 1D and 3D geoelectrical and 1D and 2D-time domain electromagnetic modelling also confirm this pattern for the Kalahari cover thickness (Ramalho et al., 2023; Francés et al., 2024). In the case of the northern section, it develops in shallow depths (10–20 m) from the beginning to the first 25 km. From this point it deepens towards the inner basin up to 35 m deep to the end of the profile.

Euler solutions (Thompson, 1982) include depths that vary from 0.76 to 30 km depth (Fig. 5). Nevertheless, these depths can be linked to the interface of the top of the KC (hundreds of meters) and the bottom of the lobes. The bottom seems to indicate the base of the mafic member of the KC. The Chiange Lobe seems to report Euler solutions at 4 km in the south, while slightly less thick in the north (~3 km). The Cuvelai Lobe reports two modes of Euler depths, one related to the lobes depth (~5 km) and the other likely associated with the upper-middle crust boundary (10–11 km). The Chibemba-E Lobe bottom presents depths that range from 4 to 5 km depth whereas the Chibemba-W lobe seems to involve shallow depths (up to 3 km). The Cahama Lobe is not well represented by Euler solutions, showing few depths (4–5 km), but the upper-middle crust boundary is well defined by solutions that range from 10 to 11 km depth. The Mutumieque area shows few solutions, probably interfered by the surficial volcanics of the Oncócua Plateau (Late Mesoproterozoic basic subvolcanic rocks) showing values of < 2 km for the bottom of the lobe. The geometry contour of the Oncócua Lobe is well defined by Euler solutions (from 2 to 4 km depth). Analogously, the Uanguembela Lobe bottom is defined by Euler solutions, presenting depth sources of 4–5 km. Main orientation of the bodies is NNW-SSE in the NE study area. The outstanding magnetic anomalies linked to the remanent bodies of the KC are smooth and homogenous to the E (Cuvelai, Chibemba E, Queulo and Cahama Lobes), dated as early stages of the KC intrusion (1.49–1.42 Ma). On the other hand, the western lobes are stretched in a NNE-SSW trend (Chiange, Chibemba W, Pocolo and Otchinjau Lobes), developed at late stages of KC (1.42–1.36 Ma). Additionally, the westernmost lobe (Oncócua) presents a N-S orientation with younger ages (1.39 Ma) (Fig. 2).

By means of the magnetic mapping we can clearly define the true eastern extent of the KC under the Kalahari sediments. The exposed area outcrops comprise 18,000 km^2, with a N-S structuring, and ca. 350 km long and up to 50 km wide. The total areas involved are ~ 53,500 km^2 with 10 lobes identified in the Angolan KC, plus the Zebra Mountains Lobe in Namibia.

4.3. Magnetic and gravimetric features and major crustal boundaries

The lineaments, understood as the linear arrangement of a geological element, inferred from the differential magnetic signature recorded by contrasted plutono-metamorphic crust of SW Angola, suggest the presence of several crustal domains (Figs. 2 and 3), also pointed out by gravimetry (Rey-Moral et al., 2022) and U-Pb zircon dating (Merino-Martínez et al., 2024). They are likely inherited from the structures that configured the Proterozoic configuration. Four domains have been classified with regard to the KC: (i) Cassinga Zone (CZ) to the east of KC (Archean to Paleoproterozoic); (ii) Central Eburnean Zone (CEZ) to the northwest of KC (Orosirian); (iii) Namibe Zone (NZ) to the west of KC (Statherian); and (iv) Epupa Zone (EZ) to the southwest of the KC (Statherian). In order to render these characteristics to the geophysical processing dealt in this work, some assumptions have been taken into account: a young, dense basaltic and thin oceanic crust is interpreted in the western domains formed during the Mesozoic Atlantic rifting, whereas an old, light and thick continental crust is considered in the eastern domains. These densities are related to the gravimetric gradient of 280 mGal throughout 600 km from the western to the eastern studied zone (Rey-Moral et al., 2022). An NNE-trending linear structure reflects the gravimetric bound-

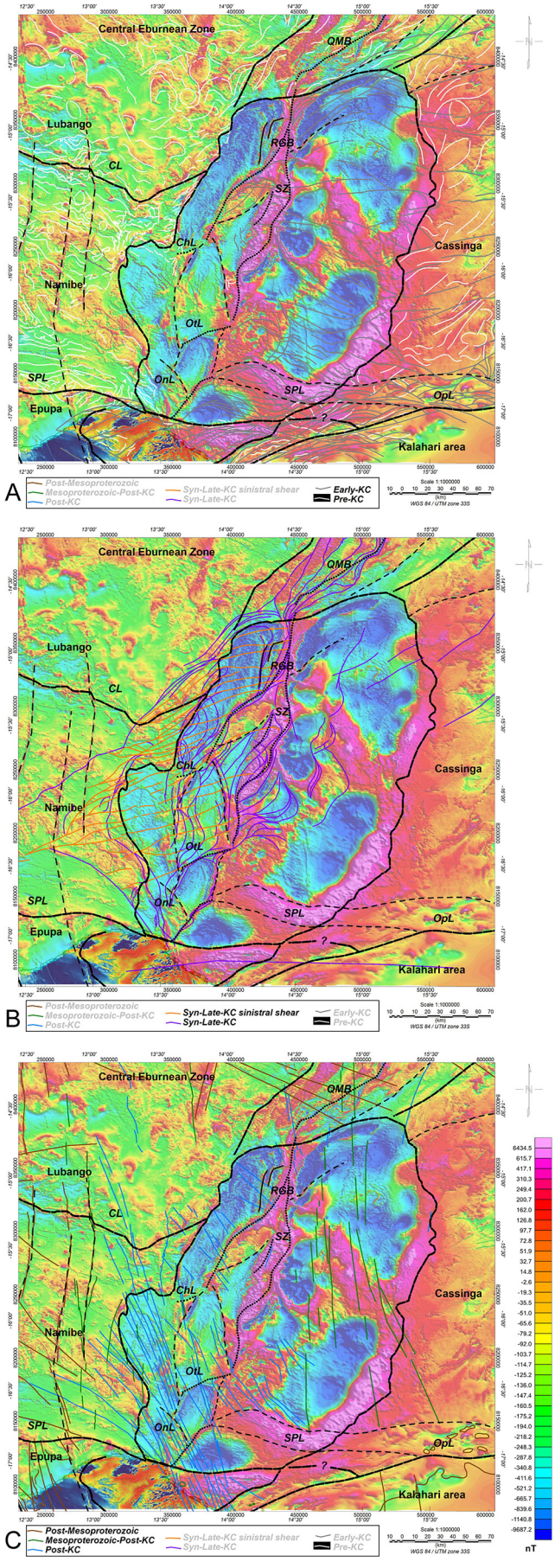

ary of these crustal portions and suggests a lithospheric weakness zone through which the KC intruded (Rey-Moral et al., 2022; Merino-Martínez et al., 2024).

The remarkable positive NNE-SSW oriented magnetic anomaly (mapped as Red granites) serves to split the eastern and western lobes of the KC. This aligned magnetic anomaly, denominated Red Granite Belt (RGB) in the north, and Shear Zone (SZ) towards the south (Fig. 2) can represent a first order shear zone between the eastern former lobes (Cuvelai, Chibemba E, Queulo, Cahama, Uanguembela and Zebra Mountains Lobes) and the western latter lobes (Chiange, Chibemba W, Pocolo and Otchinjau Lobes). The CZ presents the oldest Archean crust and the CEZ presents Paleoproterozoic Eburnean crust (Merino-Martínez et al., 2024). Euler solutions range from 0.8 to 3 km for the NE lineations enclosed in the QMB with shallow limits to the W (~1.5 km) progressively deepening to the E (2.5–3 km) (Fig. 5). The Cainde Lineament (CL, Fig. 2) is an E-W first order lineament recorded by magnetic prospecting and Euler depths (1.5–3 km). The CL is featured as a Pre-KC lineament, and it is likely deviated in the nearby KC. It is adopted as the boundary between the CEZ and the NZ. The Serpa Pinto Line (SPL, Vermaak, 1981; De Carvalho and Alves, 1990; Fig. 2) is a major ESE-WNW fault, along which the southern KC components and country rocks are thrusted northwards (Lehmann et al., 2023) in compressional sinistral kinematics. By means of the magnetic prospection in this work, it is revealed that the SPL follows the north and south limits of the Uanguembela Lobe, splitting the Angolan KC and Zebra Mountains Lobes (Fig. 2). The Opuwo Lineament (OpL, Fig. 2), which was defined by means of gravimetric and magnetic anomalies (Corner et al., 2002), was likely involved in tectono-sedientary setting of the Damara Belt of NW Namibia. It runs from the southern Zebra Mountains Lobe (Fig. 2) below the Kalahari cover eastwards. It may correspond to the Kibarian Belt continuation towards the Congo Craton eastwards and the San Francisco Craton westwards. The OpL represents a clear interruption in the magnetic record (Fig. 2), presenting a parallel trend to the Early-KC structures (Fig. 3) with deep Euler solutions that range from 3.5 to 6 km deep (Fig. 5). It is the first order structure that would separate the Kalahari area from the CZ (Fig. 2).

From north to south, some secondary lineaments were identified. The Red Granite Belt (Lehmann et al., 2023; RGB in Fig. 2) presumably constitutes a dislocated continuation of the QMB and is well shaped by means of positive anomalies in TMI (Fig. 2) and Euler solutions (Fig. 5). The Red Granite Belt (RGB) splits the early eastern and late western lobes (Fig. 2) in the northern KC. As mentioned, geometry of the lobes suggests non-deformational early setting to the E of the RGB. On the other hand, the narrow lobes located to the W of the RGB suggest deformed lobes and lineations. Shallow Euler solutions are linked to the RGB (<2 km), especially shallow west of the Chiange Lobe. Following southwards, the denominated Shear Zone (SZ) separates the eastern from the west-

Fig. 3. Structural patterns extracted from TMI derivatives in three stages. TMI common scale bar for all three stages. (A) Structures previous to KC emplacement with sigmoidal geometries to the E of the KC and NW-SE to WNW-ESE trends to the W of the KC. Early stages of KC intrusion show E-W to NE-SW orientations. (B) Syn-late KC lineaments present NE-SW orientations as the main body trend with dextral displacement evidences. Whereas other sinistral shear are recorded in ENE-WSW. (C) The absence of deformation of the NNW-SSE lineaments mainly recorded westwards suggest post-KC to post-Mesoproterozoic. QMB, Quipungo Mobile Belt; RGB, Red Granite Belt; SZ, Shear Zone; ChL, Chiange Lineament; OtL, Otchinjau lineament; OnL, Oncócua Lineament; SPL, Serpa Pinto Line; OpL, Opuwo lineament. (For interpretation of the references to colour in this figure legend, the reader is referred to the web version of this article.)

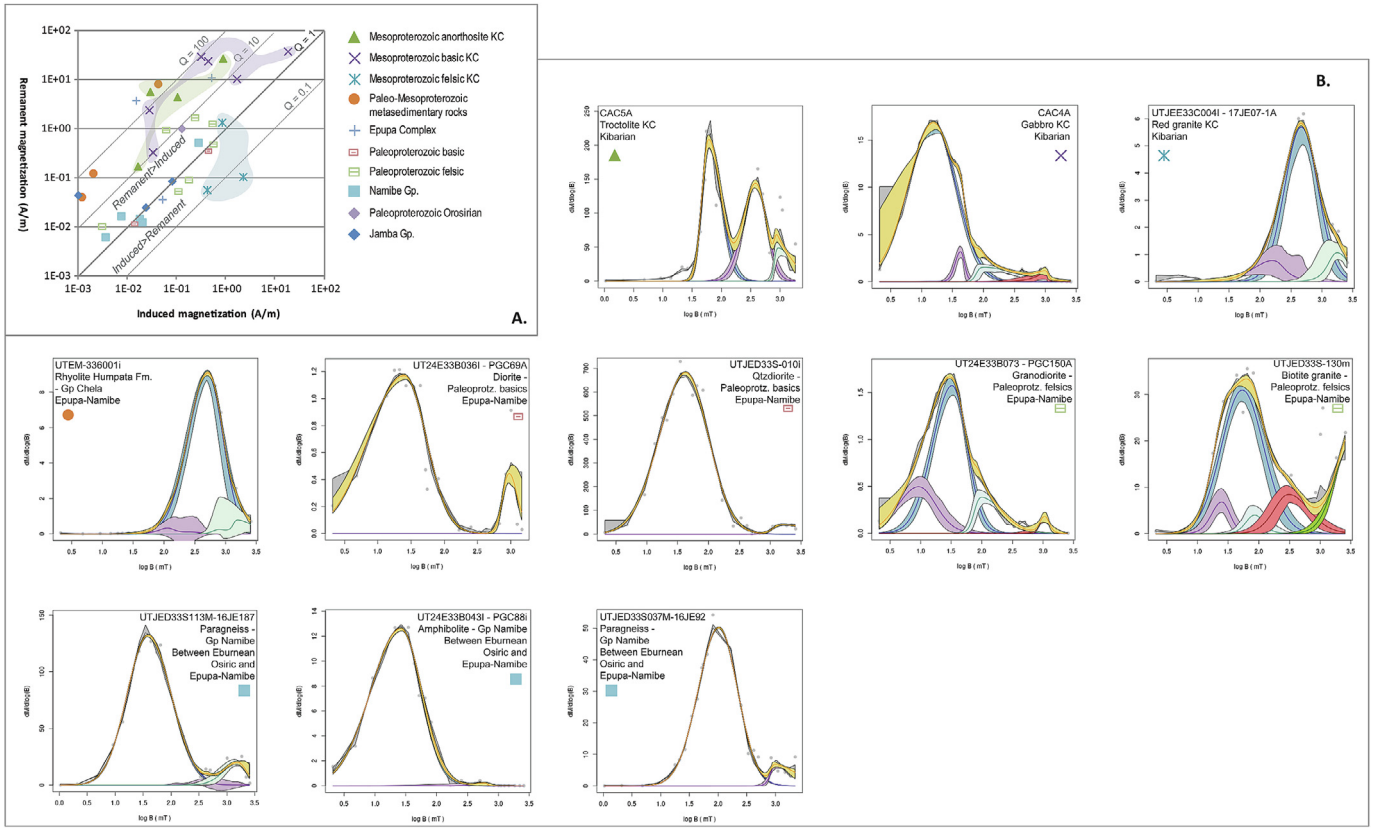

Fig. 4. Rock magnetism analyses. (A) Q ratio of the involved samples. Q > 1 indicate lithological units dominated by remanence. It is evinced that KC_Red granites are dominated by induced magnetization whereas the mafic units of the KC are dominated by remanent magnetization. (B) Isothermal Remanent Magnetization (IRM) acquisition curves obtained confirm the previous analyses where main magnetic carrier is magnetite in mafic units, whereas acid units present a mixture of high and low coercive minerals. The envelope of the sum of all magnetic species that make up the coercivity spectrum is represented in yellow with error in grey. The other colors refer to the magnetic mineral detected: dark blue for the magentite variables, purple for iron sulfides, bright blue for hematite and pink for goethite. (For interpretation of the references to colour in this figure legend, the reader is referred to the web version of this article.)

ern lobes (Fig. 2; Mayer et al., 2004; McCourt et al., 2013; Merino-Martínez et al., 2024). This lineament appears delineaded by TMI (Fig. 2) and as a lineament deducted from derivatives (Supplementary Data Fig. S4), confirmed in mapping (Rodrigues et al., 2021) (Fig. 3). Nevertheless, lineaments deducted by Euler deconvolution seem to shape the geometry of the contacts between the Red granites and anorthosites ranging between 1 and 2 km deep under the Kalahari Formation (Fig. 5). The Chiange Lineament (ChL, Fig. 2) is well depicted by means of TMI. It runs in ENE-WSW trend, contouring the southern boundary of the Chiange Lobe. Euler solutions show systematic depths under 2 km (Fig. 5). Further south, the Otchinjau Lineament (OtL, Fig. 5) describes a NE-SW trend, well defined by TMI mapping, with scarce representation by means of Euler solution, but well delineated by derivatives as *syn*-KC (Fig. 3). The OtL would present shallow Euler sources, from 1.5 to 2 km deep (Fig. 5). The ChL and the OtL traces would suggest the dextral shear of the Red granites ridges during *syn*-KC development (1370 Ma; Merino-Martínez et al., 2024). The Oncócua lineament (OnL, Fig. 2) contours the NE border of the Oncócua Lobe by means of a NW-SE trending ridge, cutting orthogonally the Otchinjau lineament. Magnetic lineaments deduced from magnetic derivatives show structural patterns that can be associated before KC intrusion, early, syn- and late KC intrusions, as well to post-KC structuration (Fig. 3). The Paleoproterozoic (Eburnean to Epupa) western crust of the KC shows magnetic lineaments from NW-SE to WNW-ESE directions (Fig. 3A). The NE-SW trend is recorded in the nearby KC, with kinematic indicators of a dextral shearing system related to the early stages of KC. The WSW-ENE lineation trend crosscuts previous and early KC lineaments, inferring late *syn*-KC deformation (Fig. 3B). The absence of deformation of the NW-SE lineaments suggests post-KC to post-Mesoproterozoic (Fig. 3C) deformation. The basement west and near to KC shows tight NE-SW structures, likely due to a change in the tectonic conditions in the western and younger lobes.

To the east of the KC, in the Archean to Paleoproterozoic Cassinga domain (2617–1971 Ma; Merino-Martínez et al., 2024), both surface structural measurements (Rodrigues et al., 2021) and magnetic lineaments suggest a dominant NE-SW structural trend linked to: (i) pre-KC structures inherited from Archean to Paleoproterozoic episodes, which sigmoidal geometries may indicate non-coaxial stages of deformation (Fig. 3A); or (ii) to *syn*-late KC lineations as consequence of contractive non-coaxial structures in late stages of KC (Fig. 3B). Early stages of KC structuration may be recorded by E-W lineations in the south of the study area, while ENE-WSW trends are observed in the north. They are probably biased by replays of fractures and crustal displacement throughout the KC development. These E-W basement lineaments are found to the NW of Namibia (Zebra Mountains) and SW of Angola (Fig. 3A). In addition, the eastern KC wall-rocks show a magnetic overlap of intense positive anomalies, possibly associated with the outstanding contribution of magnetic susceptibility derived from the intrusion of the Mesoproterozoic Red granites (Fig. 3). The trend of these granitic bodies is NNE-SSW, mimicking the main trend for the ensemble of KC mafic and felsic magmatism in its intrusion into the existent crust.

The inner lineations in the eastern lobes present NNW-SSE to NNE-SSW orientations, with no secondary deformation, likely associated to early stages of KC involvement. The Zebra Mountains

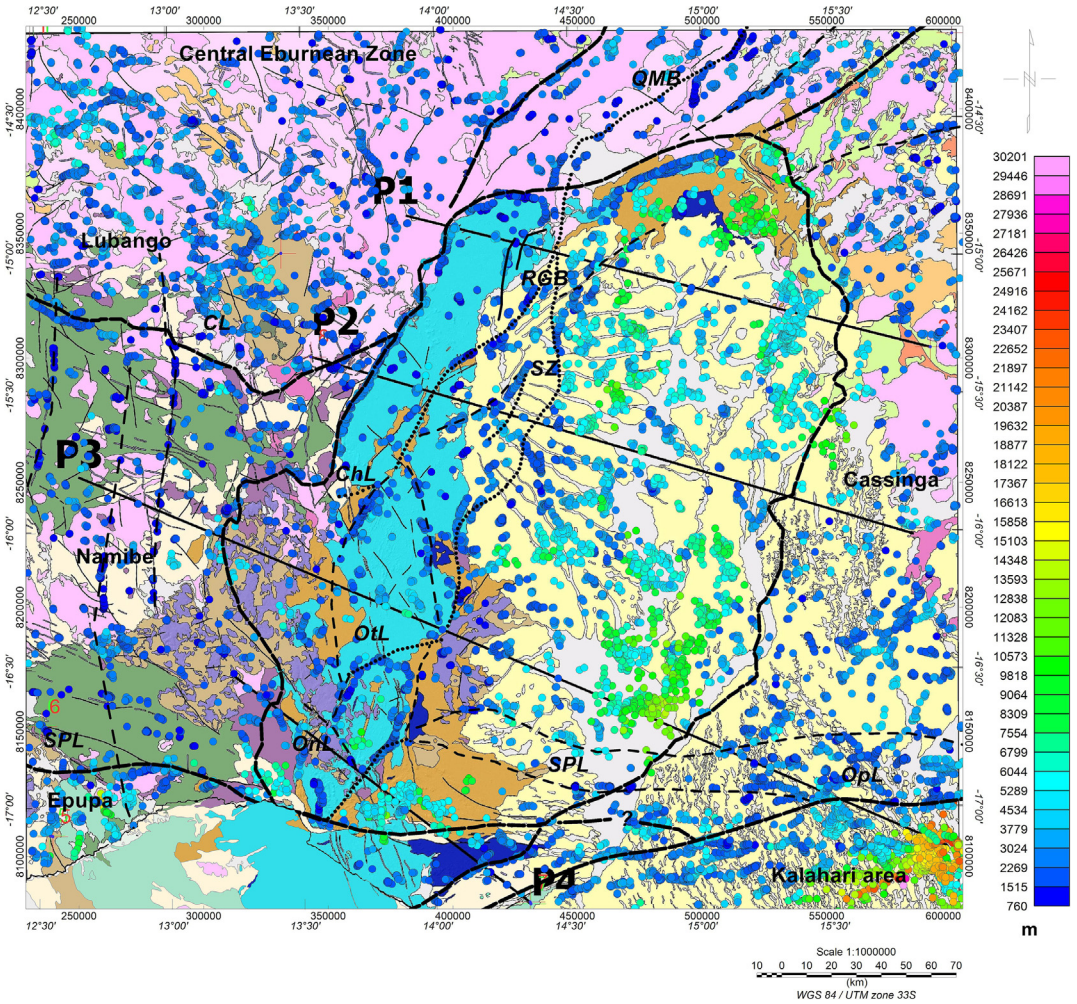

Fig. 5. Geological map and overlying depth of magnetic Euler solutions. Main lineaments are represented (QMB: Quipungo Mobile Belt; RGB: Red Granite Belt; SZ: Shear Zone; ChL, Chiange Lineament; OtL; Otchinjau lineament; OnL: Oncócua Lineament; SPL: Serpa Pinto Line; OpL: Opuwo lineament). Structural domains and modelled profiles. (For interpretation of the references to colour in this figure legend, the reader is referred to the web version of this article.)

(Namibia) and Uanguembela (Angola) southernmost lobes of the KC present a main E-W tectonic grain. Contrasted orientation with the rest of the lobes and low degree of deformation lead to considering a local tectonic regime with extensional featuring and subsequent dextral deformation (Fig. 3). Post-KC lineations present an NNW-SSE trend and Mesoproterozoic post-KC presents mainly N-S trend (Fig. 2). These trends indicate a dramatic change of tectonic setting with lineations that overlap previous KC structures. The absence of deformation of the structures and orientation could indicate an extensional regime as a consequence of the South Atlantic opening in Mesoproterozoic times.

4.4. 2.5D modelling. Structuration of KC lobes

Four regional-scale 2.5D gravimetric and magnetic profiles have been modelled to understand the deep geological configuration of the lithosphere and the in-depth configuration of the KC (location Figs. 1 and 2). The information considered for the modelling

Fig. 6. Location of the profiles on the TMI map with lobes, lineaments and structural domains differentiated. Physical parameters for the individual bodies are indicated in Supplementary Data Table 2. In all profiles, Euler solutions and structures are shown in depth. Vertical exaggeration 3. (A) TMI anomaly fitting by the model of Profile 1of 220 km long, by means of bodies which configuration is interpreted as middle-lower crust (MLC), differentiated Lubango, Transition and Cassinga crusts, Jamba Group, Paleoproterozoic metasedimentary rocks (Pom) and Undifferentieted metamorfic rocks (UmE) and felsic rocks (Pf) are intruded by KC (KC_an anorthosite, KC_gb gabbro, and KC-rg Red granites (gr)) during the Mesoproterozoic. Kalahari Cenozoic sediments (OP) cover the eastern region. (B) Profile 2 of 253 km long, fit by means of bodies which configuration is interpreted as MLC middle-lower crust, differentiated Lubango, Transition and Cassinga crusts, Undifferentieted metamorfic rocks (UmE), basic rocks (Pb), volcanic rocks (Pv) and felsic rocks (Pf) are intruded by KC (KC_an anorthosite, KC_gb gabbro, and KC-rg Red granites (gr) during the Mesoproterozoic. Kalahari Cenozoic sediments (OP) and Quaternary (Q) cover the eastern region. (C) Profile 3 of 380 km long, fit by means of bodies which configuration is interpreted as MLC middle-lower crust, differentiated Lubango, Transition and Cassinga crusts, Namibe Group (Gnm), Epupa Complex (CE) and Chela Group (Ch) Paleoproterozoic in age, are intruded by KC (KC_an anorthosite, KC_gb gabbro, and KC-rg Red granites (gr)) during the Mesoproterozoic. In turn, basic rocks of the Planalto de Oncócua (Lmb) intrude the upper crust in Late Mesoproterozoic. Kalahari Cenozoic sediments (OP) and Quaternary (Q) cover the eastern region. (D) Profile 3 of 152 km long, fit by means of bodies, which configuration is interpreted as MLC middle-lower crust, Epupa crust, Epupa Complex (CE) and Chela Group (Ch) Paleoproterozoic in age, with Paleoproterozoic intrusions of felsic rocks (Pf) and basic rocks (Pb) are intruded by KC (KC_an anorthosite, KC_gb gabbro, and KC-rg Red granites (gr)) during the Mesoproterozoic. In turn, basic rocks of the Planalto de Oncócua (Lmb) intrude the in Late Mesoproterozoic and undifferentiated metasedimentary rocksin the upper crust. (For interpretation of the references to colour in this figure legend, the reader is referred to the web version of this article.)

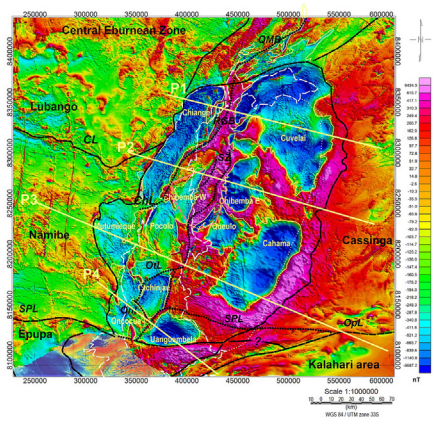

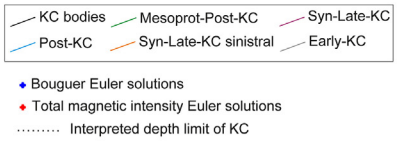

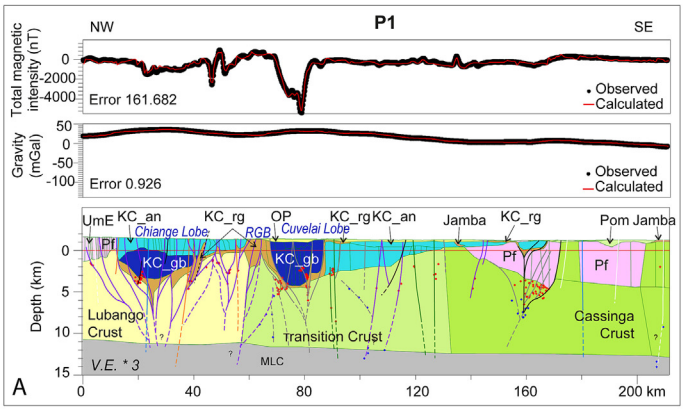

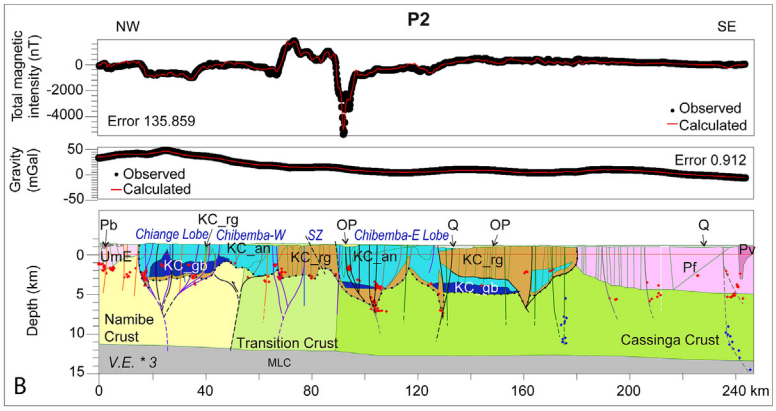

SZ: Shear Zone; RGB: Red Granite Belt

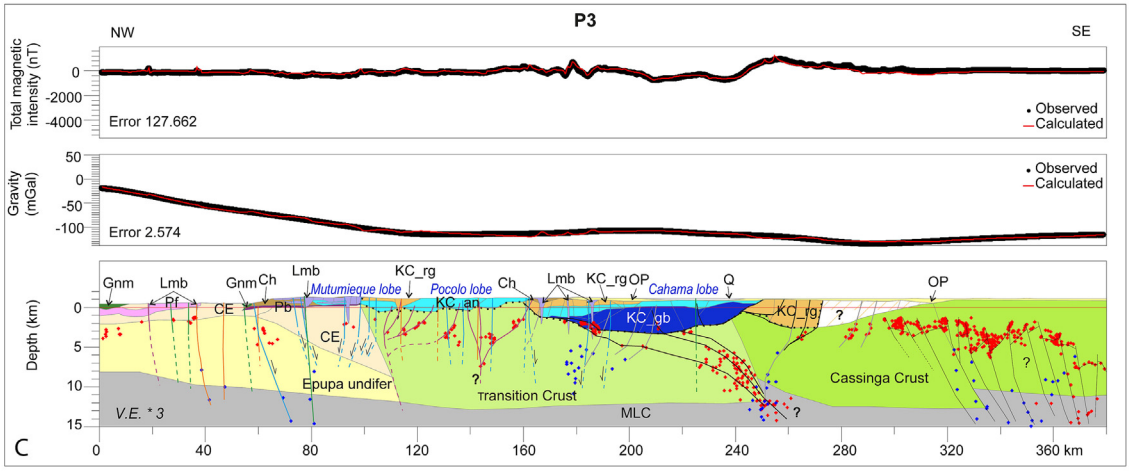

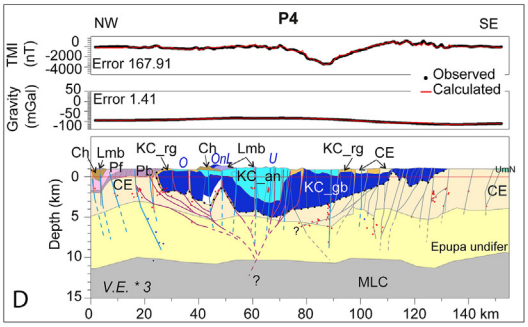

O: Oncócua Lobe; OnL: Oncócua Lineament; U: Uanguembela Lobe

includes: (1) Geological and structural information from the PLANAGEO project and the literature and geochronological information from the literature (Fig. 1); (2) TMI anomaly data from the PLANAGEO survey and Bouguer anomaly data from the BGI (Balmino et al., 2012); (3) Lineations and structures defined by TMI derivatives (Fig. 3); (4) Lower-middle crust and Moho boundaries from the CRUST 1.0 Earth-layer model (Laske et al., 2013); (5) Petrophysical measurements (Fig. 4, Supplementary Data Table 2); (6) Euler deconvolution solutions from the Bouguer anomaly (Rey-Moral et al., 2022) and from TMI (this work; Fig. 5). The Moho depth varies from 30 km in the west to 44 km eastwards. The bottom depth of the upper crust ranges from 11 km in the west to 16 km in the southeastern boundary of the study area. The limit between the lower-middle crust and the bottom of the upper crust ranges from 7 km in the west to 15 km depth in the southeastern corner of the study area (Rey-Moral et al., 2022). These depth gradients have been used to model the cross sections.

The profiles have projected coordinates: WGS84 UTM zone 33S. The results of the 2.5D modelling in the selected profiles are described as follows:

4.4.1. Profile 1

Profile 1 (Fig. 6A) crosscuts two main KC bodies, the Chiange Lobe to the west and the large Cuvelai Lobe to the east, apparently divided by Red granites and a crustal-scale structure (red Granite Belt, RGB). The properties assigned to the KC bodies are detailed in Supplementary Data Table 1. The gravimetric response changes slightly along with this profile, associated with the depth of the KC intrusions and features of the crust. The contrasted magnetic anomalies clearly suggest different magnetic properties linked to Mesoproterozoic mafic and felsic pulses, with the different response of the crystalline basement and large-scale crustal structures. In this model, the Moho boundary deepens from 39 km to 42 km and the boundary between the upper and lower-middle crust varies gently eastwards from 12 km to 13 km (Laske et al., 2013). The upper crust has been modelled considering three differential crusts progressively dense westwards (Fig. 6A). The Paleoproterozoic Lubango basement is intruded by distinct Mesoproterozoic magmas related to the KC from 12 km of the profile, irregularly extending at the crustal portions up to 168 km.

The Chiange and Cuvelai gabbro-anorthosite bodies are associated to two relative Bouguer anomaly maxima of 14 and 10 mGal, and magnetic anomalies of – 1500 nT and – 5300 nT, respectively. Between 16 km and 49 km, the Chiange Lobe presents basal gabbros (KC_gb) 3.5–5.0 km thick and considerable remanence, overlain by 0.7–2 km thick anorthosites (KC_an) (Supplementary Data Table 1 for values). The highlighted positive anomaly that splits the E (older) and the W (younger) domains seem to be linked to Red granites belonging to the RGB (Fig. 2), constituting a narrow anomaly of 10 km extent and 800 nT.

From 63 km to 190 km of the profile, most of the KC rocks are covered by Cenozoic deposits of the Kalahari Basin (OP) and Quaternary sediments (Q), with scarce outcrops between 153 km and 157 km. Nevertheless, negative TMI anomalies (–5900 nT, Fig. 2) detected from 69 km to 83 km are due to the Cuvelai gabbroic unit of the KC, unknown so far. Eastwards, a large mass of anorthositic rocks is dominant from 87 km to 155 km, thinning laterally eastwards (~ 1 km). Certain magnetic Euler solutions coincide with the bottom of the mafic magmatism of KC in both lobes (see 18–23 km and 69–91 km, Fig. 6A), between 3 and 7 km deep, while some of them lie in locations that have been interpreted as crust variations. Finally, we infer some crustal thickening of the last third Cassinga crust according to the decreasing of the gravity values. The Paleoproterozoic (Orosirian) undifferentiated metasedimentary rocks (Pom) and the Jamba Group would constitute the outcropping materials up to 219 km. At the first 50 km, transpressive duplex-type structures are modelled, which affect both the basement and the KC (Fig. 6A). A concentration of Euler solutions occurs at 160 km, indicating a possible root of the Paleoproterozoic felsic (Pf) intrusion. From 65 km to 180 km, even to the end of the profile, subvertical structures affect the basement, with possible vergence towards the SE, which could be associated with cortical fracturing processes. Post-KC philonian structures are additionally detected in 23 km and 181 km.

4.4.2. Profile 2

Profile 2 (Fig. 6B), reveals significant gravimetric and magnetic anomalies, ranging from 51 to –8 mGal and from 2000 to –5200 nT, respectively. Three main lopolith-shaped anorthosite bodies have been interpreted in this profile: Chiange, Chibemba W and Chibemba E lobes, the last older and deeper to the east (4 km in depth for the first and up to 6 km for the latter two). Large-scale structures and Red granite bodies, whose magnetic properties allowed us to satisfy the encountered anomalies (Supplementary Data Table 2 for properties) divide these lobes. At this point, the limiting structure of ancient and recent lobes is denominated Shear Zone (SZ, Fig. 2).

The model is constrained by considering a Moho depth ranging from 36 km to 38 km and an upper crust – lower-middle crust boundary from 11 km to 13 km (NW to SE) (Laske et al., 2013). The Bouguer anomaly varies from 50 to 0 mGal (from 25 km to 80 km) and from 110 km it smoothly decreases from 20 to –5 mGal related to the thickening of upper and lower-middle crust eastwards. The upper crust has been differentiated in three crustal portions (Namibe undifferentiated, Transition and Cassinga crust), with dense upper crust to the W, where a dense crust is expected derived from the opening of the South Atlantic Ocean in Cretaceous times.

At the first 26 km, the outcropping units consist of metamorphic Paleoproterozoic basement (UmE), and scarce Paleoproterozic basic plutonic (Pb) and volcanic rocks (Pv). Mesoproterozoic KC magmatic rocks subsequently crop out from 16 km to 51 km, showing a upper layer of anorthosite rocks (Chiange and Chibemba W lobes) and a lower layer of gabbros up to 4 km deep. Contrasted susceptibility and remarkable remanence (Supplementary Data Table 2) justify a total magnetic intensity amplitude of –1200 nT from 19 km to 39 km of the profile. A small outcrop of Red granites is found at 43 km, separating magmas of 1370 Ma and 1390 Ma, from 1440 Ma to 1500 Ma.

From 51 km to the end of the profile, the Cenozoic Kalahari sands, Oligocene-Pleistocene in age (OP) and other Quaternary sediments (Q) cover the crystalline basement. However, the combined magnetic and gravity signatures reveal the contribution of each source of anomalies at depth. Between 43 km and 67 km, the anorthosite body of the Chibemba W Lobe reaches up to 4 km deep. A sample of granodiorite dated at 1947 ± 4 Ma by Milani et al. (2022) immediately south of this profile suggests the possibility of finding an older Eburnean crust beneath this anorthosite body and, therefore, included as transitional crust in the modelling.

Further east, a large mass of NNE-trending Red granites matches the strong positive magnetic anomaly found between 67 km and 91 km (2000 nT), has been named Shear Zone (SZ in Fig. 2). The contrast with gabbro-anorthosite KC is accentuated at 90–95 km, where a strong negative magnetic anomaly reaching –5200 nT is found, implying a subvertical structure that separates high remanence bodies to the east, opposite to the Red granites (Supplementary Data Table 2). Actually, from 90 km to 180 km, distinct KC anorthosite and felsic units are modelled in the upper crust, conforming the Chibemba E Lobe, anorthositic up to 5 km deep, and the southern end of the Cuvelai Lobe, in this section constituted of the halo of granitic rocks (~2.5 km thick) (Fig. 6B). The easternmost body is characterized by a layer (1–2

km) of anorthosite, although the gravity relative maximum of 10 mGal amplitude suggests an underlying basal gabbroic unit 1–2 km thick.

The Bouguer anomaly slightly decreases from 190 km to the end of the profile, suggesting a thickness increase of the Cassinga crust, whose bottom reaches 13 km depth. Paleoproterozoic felsic igneous and eastwards Paleoproterozoic volcanic rocks (Pf and Pv) are modelled at the end of the profile. The Euler solutions between 3 and 7 km depth support the rooting of the KC bodies. Euler solutions in the last 50 km of the profile show apparently extensional structures, which modelling suggest extension in the E domain of the KC. At the beginning of the profile (first 90 km), narrow bodies interpreted as transpressive structures would be linked to the second stage of emplacement of the KC, where basement is involved. Late-KC structures are interpreted in the west (Fig. 6B) by Euler solutions and magnetic lineations (Fig. 3). Post-KC dikes are mainly recorded in the E, from 120 km to 180 km (Rodrigues et al., 2021).

4.4.3. Profile 3

Profile 3 (Fig. 6C) includes two large KC bodies, the Pocolo Lobe to the west and the Cahama Lobe to the east, separated by anomalies of intermediate intensity. The properties assigned to the KC bodies are in Supplementary Data Table 2. This model considers a Moho depth ranging from 34 to 38 km and the upper crust and lower-middle crust boundary from 8 km to 11 km (Laske et al., 2013). The upper crust is laterally structured in three sectors, as described in previous profiles (Fig. 6C). A decrease in the Bouguer anomaly (270 km to the end), together with marked change of the magnetic signature, outset the thicker Cassinga crust.

The shallow part of the Epupa crust is occupied by the Epupa Complex (CE), cropping out between 38 km and 57 km of the profile, but also interpreted in depth up to profile 100 km. The magnetic Euler solutions fit with the bottom of the Epupa Complex (CE). Low grade Paleoproteroroizoc to Mesoproterozoic metasedimentary sequences (Ompupa Group, Ch) together with interstratified late Mesoproterozoic mafic subvolcanic materials (Lmb, ca. 1.1 Ga; Salminen et al., 2018) are arranged horizontally from 57 km to 100 km. Some of the vertical gravimetric Euler solutions found at depth would be related to the deep crustal faults and the geometry of the feeding conduits of the basic (sub-)volcanic rocks.

The KC complex occupies the middle part of this profile. The KC anorthosites and gabbros cause a long wavelength (120 km) gravity relative maximum of 10 mGal amplitude. The distinct KC bodies are structured following a lopolith shape, characterized by a thin layer of anorthosites (0.5–1.5 km thickness), which is mostly compose the middle- to late-KC. Mutumieque basalts at the northwest seem to mask a deep lobe. The Pocolo Lobe extends from profile 120 km to 163 km. The Cahama Lobe includes a thick layer of gabbros between profile 180 km and 250 below the anorthositic layer. The contrasted magnetic properties would justify magnetic anomalies of ~ 1600 nT (see Fig. 2; 235–252 km). Red granites associated to KC crop out between 100 km and 120 km, linked to a magnetic anomaly of 250 nT amplitude. Syn- to late KC subvertical structures are likely related to the intrusion of the western segment of the KC. Further east, some late Mesoproterozoic metasedimentary rocks of the Cahama Formation (Ch) and late Mesoproterozoic mafic volcanics (Lmb), cropping out between 160 km and 170 km, are likely overlying the continuation of the early- middle-KC magmatism of the Cahama Lobe. Cenozoic Kalahari sands (OP) are exposed at the end of the profile. Nevertheless, the magnetic and gravity data support the presence of large KC bodies below this sedimentary cover. Magnetic Euler solutions are associated with the basal boundary of the KC, mainly formed by bodies of gabbros. Other gravimetric Euler solutions (180 km) would represent deep faults through which the late Mesoproterozoic dykes ascended to the surface. It is interesting to note that the remarkable concentration of gravimetric and magnetic Euler solutions (between 5 and 15 km of depth) between 220 km and 260 km may be associated to the limit between crustal domains (Transition and Cassinga crust) and also a weakness zone (crustal detachment?) for the magma feeding of the KC. The > 2500 nT magnetic anomaly at 260 km is resolved by modelling Red granites under the Kalahari sediments. By joining the gravimetric and magnetic modelling, the new southeastern limit of the KC extends ~ 20 km more than the previous interpretation (Rey-Moral et al., 2022). Post-KC subvertical structures and lineaments widely crosscut all the crustal rocks described above.

4.4.4. Profile 4

Profile 4 (Fig. 6D) extends to the south of the N-S Oncócua Lobe, dated at 1371–1392 Ma and the older E-W structured Uanguembela Lobe dated at 1434–1438 Ma (Fig. 2). The properties assigned to the KC bodies are in Supplementary Data Table 2. In this profile, the Moho depth remains almost flat (37 km) and the upper and lower-middle crustal boundary range from 11 km at the NW to 12 km at the SE (Laske et al., 2013). The Epupa undifferentiated crust formed the upper crust of this profile, underlain by the plutonic-metamorphic Epupa Complex. The beginning of the profile is characterized by the outcropping metasedimentary rocks of the Ompupa Group (Ch), intruded by late Mesoproterozoic mafic subvolcanic (Lmb) materials (1127 ± 8 Ma; Salminen et al., 2018). A link between the deep magnetic Euler solutions and the feeder conduits of this mafic magmatism is depicted in the profile. Most of the basement materials found in the southern part of the KC are related to Epupa event units, dated between 1767 Ma and 1830 Ma.

The KC rocks occupy most of the profile extent, cropping out almost continuously between 27 km and 133 km, associated with a Bouguer anomaly maximum of 12 mGal and a minimum magnetic anomaly of −3400 nT. To fit the anomalies, we model a thick gabbroic layer underlying an upper anorthosite unit, rather thin south in the Oncócua Lobe and up to 5 km thick in the Uanguembela Lobe. Some thin layers of felsic materials are found between gabbro-anorthositic pulses favored by detected structures by derivatives (Fig. 3). Both lobes seem to be separated by a crustal-scale structure, the Oncócua lineament (OnL). Some magnetic Euler solutions coincide with the bottom of the KC at the beginning of the profile and shape the morphology of the syn- to late lineaments displayed in the profile, probably responsible for the magma ascent and emplacement of the KC episodes. The outcropping Red granites are associated with magnetic anomalies of short wavelength (~ 3 km; see 24, 38, 76, 95 and 105 km of the profile).

The Epupa Complex (CE) crops out at the end of the profile, partially covered by other Neoproterozoic metasedimentary rocks (UmN), overlying the crystalline basement of SW Angola and NW Namibia (Fig. 1). Between 98 – 102 km and 107 – 112 km, the outcropping CE is irregularly found between Mesoproterozoic granites and gabbros (see 104 km of the profile). This crustal faulting also affects the underlying early- to middle Mesoproterozoic gabbros and compartmentalizes the southeastern half of the profile. For that reason, these magnetic lineaments have been interpreted as early KC structures.

4.5. 3D modelling

Three MVI susceptibility models were performed to better understand the KC lobes geometry and their geological configuration in depth (Fig. 7). For each model we created several isosurfaces, represented by different ranges of MVI susceptibility values (S.I.) that allow us to characterize the Mesoproterozoic rocks that form the KC, specifically anorthosites, mafic magmatism

(gabbros) and felsic magmatism (Red granites). All observed MVI susceptibility values are compatible with the 2.5D modelling and with measured magnetic properties (k, NRM, Supplementary Data Table 2).

4.5.1. Chiange-Chibemba model

From the Chiange-Chibemba amplitude of magnetization voxel we extracted two sections (S1_CC and S2_CC) (Fig. 7 for location). These sections are represented by different MVI susceptibility values (S.I.) that characterize the KC rocks: anorthosites (0.002–0.04 S. I.), gabbros (0.04–0.2 S.I.) and Red granites (0.002–0.04 S.I. and 0.06–0.5 S.I.) (Fig. 7A, Supplementary Data Fig. S1, to fully view the figure use an advanced PDF viewer).

(1) S1_CC section

S1_CC section runs from NNW to SSE for 67 km (Fig. 7A). Approximately after 60 km the KC rocks are covered by the Kalahari Formation KC anorthosites isosurfaces were interpreted between 17 – 44 km and 51 – 58 km. The Red granites appear dominantly between 44 – 51 km and 58 – 67 km. Between 58 km and 67 km is likely registered the interference of Red granites with Paleoproterozoic felsic rocks, with no possibility to discriminate them at end of the profile 1 (Fig. 6A). KC gabbros appear preferentially in depth underlying the anorthosites between 18 km and 37 km with thickness between 0.5 and 5.5 km. These bodies seem to be responsible for the negative magnetic anomalies detected in the S1_CC section (Fig. 7 for location). Sub- or outcropping anorthosites thickness ranges from 1.5 to 7 km. Red granites are related to positive magnetic anomalies and their thickness varies between 2.5 and 7 km. Characteristic remanence variation resulting from MVI inversion can be observed (Fig. 7 A1, A2), where we present the distribution of magnetization vectors near S1_CC section. Dipping of the bodies helped us to determine contact zones between early and late pulses. E dipping faults are linked to the late KC emplacement in the first 20 km of the S1_CC profile, where KC intrusion occurred (Fig. 7A, Supplementary Data Fig. S1). The pulses of the late KC are associated with flower structures at 25–30 km and 37–42 km in the Chiange Lobe. From 45 km to 53 km it looks like the late KC lobes overlaid and were thrust over the early KC lobes. Towards 61 km and 63 km the boundary between the early and late KC intrusions is interpreted.

(2) S2_CC section

S2_CC section runs from NNW to SSE for 98 km (Fig. 7A). After 57 km, the KC is covered by the Kalahari Formation. In the S2_CC section, Mesoproterozoic KC anorthosites were interpreted between 15 km and 67 km. At 39–41 km granites are exposed, generated in the second KC emplacement episode. Magnetic inversion probably does not detail the featured isosurface related to Red granites masked by the intense isosurfaces resulting from the inversion of the gabbros around 40 km (Fig. 7A). At 41 km, the boundary between the late 1.39–1.37 Ma KC pulses, to the E, and the early 1.5–1.44 Ga KC pulses, to the W, would be established. This boundary is described as the NNE trending Red Granite Belt (RGB, Lehmann et al., 2023). A marked contrast between intensely positive anomalies linked to Red granites of the RGB (Figs. 2 and 7) and remanence linked to the mafic rocks would constitute a main shear zone. Red granites between 67 km and 92 km are linked with another major shear zone (SZ, Figs. 2 and 7), probably interfered with the Paleoproterozoic felsic rocks dated at 1947 Ma (Milani et al., 2022). We, therefore, suggest the existence of relict Paleoproterozoic basement between the early and late KC pulses, between the SZ structures, shearing that would reach crustal depths. KC gabbros are present preferentially in depth underlying the anorthosites between 15 km and 21 km, 33 km and 42 km and 92 km and 96 km of S2 section. Gabbros thickness varies between 5 and 6 km and is characterized by high values of susceptibility (0.04–0.2 S.I.) and very high remanence. The anorthosites thickness ranges from 1.5 to 7 km, which rocks present a medium–high susceptibility (0.002–0.04 S.I.) and low remanence. Red granites are related to positive magnetic anomalies, and their thickness ranges from 5.8 to 7 km (Fig. 7; Chiange-A). Red granites are characterized by high susceptibility (0.06–0.5 S.I.) and low remanence, whereas high remanence is detected in contact zones between negative and positive magnetic anomalies (Fig. 7 Chiange-A). The MVI susceptibility model and extracted sections (S1 and S2) are coherent with 2.5D modelling and analyzed rocks. Generally, KC is characterized by a unit of gabbros located in depth overlain by a layer of anorthosites and a Red granites body located on the SE end of the sections. Nevertheless, the MVI model shows some discrepancies with 2.5D model, particularly in the maximum thickness of the interpreted source bodies, probably related with the presence of host rocks with magnetic susceptibilities similar to the ones that characterize the rocks associated with KC.

4.5.2. Cuvelai model

From the Cuvelai amplitude of magnetization voxel we extracted one section (S1_Cuv) located along the P1 profile (Fig. 7 for location). This section is represented by the same MVI susceptibility ranges as in the Chiange-Chibemba model, which characterizes the KC Mesoproterozoic rocks in this region (Fig. 7B, Supplementary Data Fig. S2, to fully view the figure use an advanced PDF viewer).

(1) S1_Cuv section

S1 section runs from NNW to SSE along 108 km (Fig. 7B). In this section, the KC rocks are covered by the Kalahari Formation. Red granites occur between 0 and 13 km and between 30 km and 40 km with maximum thickness of 6 km, which magnetization is particularly intense on contact zones between negative and positive anomalies. KC gabbros occur from 13 km to 19 km, which thickness varies between 6 and 7 km. KC anorthosites are located between 19 km and 30 km and between 40 km and 103 km and show a maximum thickness of 7 km (Fig. 7B). Like in the Chiange-Chibemba model, intense positive anomalies zones are probably related to the contact between anorthosites and Red granites on the shear zone that separates Chiange and Cuvelai lobes (Fig. 7). However, in other areas, the Red granites have a medium–high susceptibility (0.002–0.04 S.I.) and low remanence.

On the NNW segment of the section, KC is characterized by two source bodies formed of Red granites and gabbros, which contact probably is the primary structure of the Red Granite Belt with sub-vertical dipping. Structuration in the S1_CC, where the Chiange Lobe is involved, reveals the late stage of intrusions with narrow bodies and sub-vertical structures, compatible to transpressive positive flower structure configurations with late KC pulses overlapping or thrusting over early KC bodies. On the other hand, the structural arrangement of bodies in the eastern S1_Cuv (Fig. 7B), where the Cuvelai Lobe is involved, suggest extensional geometries formed of anorthosites, with less dipping faults than the Chiange Lobe. High volume of anorthosites (between two and three times more than the western lobes) with low density of lineaments suggests a relative extension despite of the general collisional setting. However, one more time the MVI susceptibility model shows some discrepancies with the 2.5D model in the maximum thickness of the interpreted source bodies, probably related to the similarity in the magnetic properties of host rock and of KC rocks.

4.5.3. Oncócua-Uanguembela model

From Oncócua-Uanguembela amplitude of magnetization voxel we extracted one section (S4_OU) along part of P4 profile (Fig. 7). This section is represented by MVI susceptibility values (S.I.) that characterize the Mesoproterozoic KC rocks, anorthosites (0.002–0.04 S.I.), gabbros (0.04–0.2 S.I.) and Red granites (0.002–0.04 S.

I.) (Fig. 7C, Supplementary Data Fig. S3, to fully view the figure use an advanced PDF viewer).

(1) S4_OU section

S4_OU section runs from NW to SE for 117 km (Fig. 7C) and KC rocks crop out along the section. KC anorthosites crop out between 29 km and 35 km, 40 km and 75 km, and 81 km and 90 km, which thickness ranges from 2.5 to 7 km. Red granites crop out between 22 km and 29 km, 35 km and 40 km, 75 km and 79 km, and 90 km and 108 km; their thickness ranges from 4.5 to 7 km. KC gabbros occur preferentially at depth, underlying the anorthosites between 24 km and 29 km and 77 km and 117 km of the section with thickness that varies between 2 and 7 km (Fig. 7C). Structures interpreted in the S4_OU inversion are linked to the NNW-SSE general trend of the Oncócua Lobe and NNE-SSW of the Otchinjau Lobe, both belonging to the late KC intrusions. Both lobes are separated by compressive structures of the lobes (1.39–1.37 Ga). 66 km likely represents the boundary between the early and late pulses of the KC. Further east, the KC structure adopts west-east orientation due to the replay of transpressive processes that make the KC thrust northwards, along the Serpa Pinto line (Lehmann et al., 2023). Such structuration causes continuous W-E anomalies at the bottom of the profile at 75 km.

The Oncócua-Uanguembela model and extracted section (S4_OU) are coherent with 2.5D modelling but with some differences. Probable causes for this thickness discrepancy are the similarity in the magnetic properties of host rock, and of KC rocks and similar range of susceptibility for anorthosites and Red granites that can complicate the interpretation of the results.

5. Discussion

5.1. Magnetic mineralogy in KC terrains and basement

Anorthosites of the KC present medium values of susceptibility (0.0040 S.I.) with high remanence (7.6518 A/m), whereas density is relatively higher than its background (2749 kg/m^3). Laboratory measurements of the mafic magmatism of the KC (mainly gabbros) reveal medium–high magnetic susceptibility (0.0150 S.I.) and very high remanence (29.3330 A/m) and density (2810 kg/m^3). On the other hand, the felsic magmatism associated to the KC (Red granites) presents relatively higher values of magnetic susceptibility than the other KC units (0.0272 S.I.), and very low remanence (0.0999 A/m), and low density (2644 kg/m^3), values that allow for us to establish a marked contrast of properties to be transferred to the scope of modelling.

The magnetic signatures described by IRM acquisition curves allowed us to classify the KC lithostratigraphic units and wall rocks. The wall rock of the Namibe Group (2 Ga) presents a magnetization mainly carried by magnetite with minimal coexistence of high coercivity minerals in the case of igneous protolith. The rhyolites of the Chela Group merely present high coercive minerals. Paleoproterozoic felsic rocks show numerous magnetic carriers (more than 50% magnetite with variable content of low and high coercivity minerals) whereas Paleoproterozoic basic rocks present a prevalence of magnetite. Assorted magnetic carriers are observed in the KC units, which is reflected in their magnetic signatures: basic units of the KC present a main content of magnetite, associated to the high values of magnetic susceptibility and very high remanence (Fig. 1). On the other hand, altered anorthosite/troctolite present similar low and high coercive minerals with moderate values of susceptibility and remanence. Red granites present mainly high coercive minerals, as hematite, showing high susceptibility and very low remanence.

The mineralogical assemblage of KC non-altered anorthosite presents plagioclase, with subordinate olivine, pyroxene and accessory magnetite and ilmenite (Lehmann et al., 2023). Magnetite as an accessory mineral in KC mainly carries the remanence and as main remanence carrier in domain structures of single-domain (SD) particles and may dominate the magnetic recordings more efficiently than other ferromagnetic minerals (Piper, 1974). This unaltered anorthosite is linked to a fresh black fraction of the anorthosite whereas altered anorthosite is rather white (Drüppel et al., 2007), providing the characteristic Zebra Mountains facet, with E-W ridges of dark and valleys of white anorthosite. The altered anorthosite may lead to epidote group minerals, sericite, actinolite, carbonates and albite, providing the whitish appearance. Ferromagnetic minerals can be altered to chlorite (Lehmann et al., 2023), as effect of weathering, chlorite being paramagnetic and therefore weakly magnetic. It is pointed out that the unaltered anorthosite is olivine-bearing, whereas metasomatized olivine-poor fraction produces the liberation of Fe-Ti inclusions. Therefore, depending on the degree of alteration, KC anorthosite presents lower susceptibility and remanence than KC gabbro (as measured and modelled in the present study; Supplementary Data Table 2). On the other hand, rock forming minerals of the Red granites are K-feldspar, quartz, biotite, plagioclase and hornblende (Milani et al., 2022), which featured red colour is due to the iron oxide inclusions as hematite (Lehmann et al., 2023), confirmed by IRM analyses of this study (Fig. 4). Red granites are therefore dominated by very high susceptibility mainly carried by high coercivity minerals and low remanence, which would explain this strong contrast of anomalies versus strong remaining magnetizations of basic KC, especially in gabbros and anorthosites. Magnetite is a ubiquitous accessory mineral in troctolitic anorthosite and constitutes the major magnetic carrier of the KC up to 20% of the rock (Piper, 1974). In addition, we propose that mafic rocks of the KC are dominated by remanent magnetization ($Q > 1$, Fig. 4A), with magnetite being primarily responsible for remanence of the dark troctolitic anorthosite, where it appears as discrete grains and as thin rods in the plagioclase (Ashwal, 1993). This high remanent magnetization of reverse polarity allows an optimal magnetic mapping definition of KC lobes (Fig. 2).

5.2. Magnetic structure of the SW Angolan crust

The contrasting magnetic behaviour of the plutono-metamorphic crust of SW Angola and the distinct magnetic lineaments that characterize the area suggest the existence of several crustal domains structured in assorted directions. Such opposite directions are detected in a quick view of the magnetic image: KC lobes with high remanence and negative magnetic polarity bordered by Red granites with normal polarity. Large-scale crustal lineaments are clearly depicted in the magnetic field, probably derived from inherited Proterozoic structures. Differences in the crustal properties of the basement surrounding KC have been previously detected. Rey-Moral et al. (2022) noticed a gradient of the Bouguer anomaly from W to E, showing highly positive Bouguer values on the Atlantic margin (+250 mGal) which differ from those negative values towards the northeast of the study area (−30 mGal). In addition, a recent research work of Merino-Martínez et al. (2024) reveals the distinct crustal domains of the crystalline basement of SW Angola and NW Namibia. These structural domains are clearly depicted by magnetic prospecting (Fig. 2).

Different magnetic signatures are recorded in the basement on both sides of the KC. The Paleoproterozoic (Eburnean to Epupa) western crust of the KC is characterized by medium to low magnetic intensity values (−100 to −150 nT), showing magnetic lineaments varying from NW-SE to WNW-ESE orientations (Fig. 3), similar to the striking fabrics described in the surface structural measurements (Merino-Martínez et al., 2022). Some positive anomalies (up to 250 nT) found in this area are related to the pres-

ence of Paleoproterozoic felsic and mafic igneous rocks, dispersed within the dominant metasedimentary and metaigneous basement. On the contrary, to the east, the Archean to Paleoproterozoic Cassinga crust (2617–1971 Ma; Merino-Martínez et al., 2024) presents high magnetic intensity values up to 150 nT (Fig. 2), constituting the magnetic background of the studied area. Both the surface structural measurements and deep magnetic lineaments suggest a dominant NE-SW structural trend, disturbed to NNW-SSE and NNE-SSW directions near the KC boundary (Fig. 3; Merino-Martínez et al., 2022). In addition, the eastern KC wall rocks show a magnetic overlap of intense positive anomalies, possibly associated with the outstanding contribution of magnetic susceptibility from the intrusive bodies of the Red granites (Fig. 2), reaching values of magnetic intensity up to 6000 nT (Fig. 2). According to Rey-Moral et al. (2022) and Merino-Martínez et al. (2024), the western and eastern crustal domains surrounding the KC are separated by a large-scale NNE-SSW trending structure, that possibly represents a lithospheric weakness zone, through which the KC intruded. This structure was previously described by Torquato (1977) as the Quipungo Mobile Belt, possibly formed during Late Paleoproterozoic times (during the Namib event, i.e. ~1670 Ma).

5.3. KC limits and emplacement constraints

As a whole, the Kunene Complex conforms to an ovoid-shaped plutonic structure, showing the maximum elongation axis following a NNE-trend, comprising a total area of 53,400 km^2, being extraordinarily above the previously known KC outcropping area (42,500 km^2 suggested by Rey-Moral et al., 2022). However, by means of this work the igneous complex is clearly composed of individual bodies, forming a set of separate plutons elongated in distinct directions, mainly oriented in an NNE-SSW-trend, but also varying towards NW-SE and E-W directions (Fig. 2). The most-important gabbro-anorthosite bodies of SW Angola are distributed in eleven ellipsoidal lobes, three cropping out (Chiange, Pocolo, Otchinjau lobes), other three partially cropping out (Chibemba-W, Oncócua and Uanguembela lobes), but other four not explored so far, are identified here under the Cenozoic cover (Cuvelai, Chibemba-E, Queulo and Cahama lobes) in Angola, plus the Zebra Mountains Lobe in Namibia. According to the 2.5D modelling, the dimensions of these individual lobes range from 20 to 80 km long and 9 to 35 km wide (Table 2). Lobes are generally larger and thicker in the E region that in the W, from 3 to 5 km depth, which geometries would add up to an extensional scenario, whereas the W region, depths from 1.8 to 4.4 km would suggest a modified compressive setting (Table 2). The extensional or compressional settings are interpreted from geometries of the anomalies associated with KC lobes and the orientation lineaments affecting KC lobes and basement.

The KC involved units would intrude in the Congo Craton during the main Kibarian event s.s. (1000 – 1400 Ma) according to Tack et al. (2010). This intraplate event with a polyphase magmatic system is evidenced by the ages obtained from KC lobes. The emplacement of the distinct pulses occurred episodically, evolving westwards through lateral-driven forces within a regional NNW-SSE contractional context. Most of the early pulses (1534 Ma to 1420 Ma) are located in the sediment covered eastern segment of the Angolan KC and in scarce variably deformed granite rocks in NW Namibia, while the later pulses (1410–1340 Ma) are mostly found in the NW and SW exposed boundaries (Fig. 2). This geochronological arrangement lead Merino-Martínez et al. (2024) to suggest distinct domains within the KC (early- to middle KC to the east, and middle- to late-KC, to the west), favored by the episodic emplacement and rejuvenation of the complex westwards. Regarding the magnetic signature, it is interpreted that the intense positive anomalies are derived from the intrusion of Red granites (1.4–1.45 Ga) in early stages of KC.

The Red granites seem to split the Cuvelai/Chibemba/Queulo/Cahama lobes to the east and the Chiange/Pocolo/Otchinjau/Oncocua lobes to the west with NNE-SSW trend, throughout the RGB and the SZ. The RGB is probably related to the ascent of partially molten crustal materials in NNE-SSW linear structure (Lehmann et al., 2023). In the root of the profile 3, a concentration of Euler solutions could inform about the limit between crustal segments that could be developed as trigger point (crustal detachment?) for the magma feeding of the KC. This would correspond to a complex transpressional and extensional system evolving from the early Mesoproterozoic to the early Neoproterozoic. The southern Uanguembela Lobe (Fig. 2) presents intermediate ages (1.43 Ga). It is interesting to note that most of the gabbro-anorthositic lobes found to the east of the KC show smooth and almost homogeneous magnetic anomalies, while those found in the western segment reveal more flexed magnetic lineation. The magnetic lineaments found in this western sector shape an internal morphology composed of subvertical anorthosite (± gabbro) and granite sheets, distributed parallel to the plutonic boundaries. In addition, the eastern part of the KC lobes covers an approximate width between 150 and 100 km, whereas the western segment does not reach 50 km width. Few physical properties differences have been detected between lobes, although greater susceptibility and remanence are detected in the southern KC gabbros (i.e. Uanguembela Lobe) with respect to the northern lobes (i.e. Chiange or Cuvelai lobes), while this gradation in the anorthosites is the contrary, with greater susceptibility and remanence in the north. Such differences are not noticeable in the Red granites. On the other hand, no relevant changes are detected in the density properties except for the mafic rocks of the south (Chahma and Uanguembela lobes), which have slightly lighter densities that in the northern lobes. A third stage of KC formation could be differentiated westwards, with the non-deformed and N-S oriented Oncócua Lobe.

The gabbro-anorthosite bodies are intimately linked to granites, as also suggested by the published U-Pb crystallization ages (see reviews of Lehmann et al., 2020; Milani et al., 2022; and Merino-Martínez et al., 2022). Mesoproterozoic-felsic rocks of SW Angola and NW Namibia are dated between 1534 Ma and 1342 Ma, while the U-Pb crystallization ages of the gabbro-anorthositic rocks are comprised between 1500 Ma and 1344 Ma, strongly suggesting a close spatio-temporal relationship. Large positive magnetic anomalies (from 1000 to 6500 nT) are found surrounding the gabbro-anorthositic KC bodies, that have been interpreted as associated with these Mesoproterozoic felsic magmas. Intense positive anomalies apparently divide the massif in NNE-SSW direction into two segments (Fig. 2). These anomalies are associated with a set of strike-slip structures along with exposed Mesoproterozoic granitoid magmas and scarce plutono-metamorphic basement materials. Other minor positive anomalies are located between and within gabbro-anorthosite bodies, following a similar structural arrangement, which would evidence the linkage between partial melting processes in the lower crust and the ascent of deep mantle-derived melts aided by magma buoyancy through viscosity and density differences (Dobmeier, 2006). In fact, the presence of mangerite and other granite dykes, dated between 1378 Ma and 1371 Ma (Mayer et al., 2004; Lehmann et al., 2020; Milani et al., 2022), found in the plutonic boundaries of the Chiange and Oncócua lobes (in the NW and SW segments of the KC), showing structural trends and deformational textures parallel to the plutonic boundaries (Merino-Martínez et al., 2022; Milani et al., 2022; Lehmann et al., 2023), even intruding other previous KC pulses (granite gneisses and older anorthosites dated between 1500 Ma and 1440 Ma; Bybee et al., 2019; Lehmann et al., 2020), would suggest intrusion favored by transpressional processes in a long

lasting episodic magmatic system. In fact, the morphological and structural arrangement of the KC lobes, according to the different direction of the elongation axis, varies from NNE-SSW to NNW-SSE in the Angolan KC to E-W in the southern Angolan KC and Namibian KC (Zebra Mountains; Fig. 2). Considering the macrostructural elongation both the NNE-trending Quipongo Mobile Belt (QMB) and the E-trending Serpa Pinto Line (SPL, Fig. 2) seem to represent major planes of structural weakness that facilitated the ascent and emplacement of KC magmas during the Mesoproterozoic (Rey-Moral et al., 2022). The QMB (Fig. 2) could represent the precursive suture of the KC and separator of the Central Eburnean Zone (CEZ) and Cassinga Zone (CZ).

The KC lobes are synchronous with the adjacent granites and we propose that the mafic magma provided the heat for crustal melting that generated the granitoids by crustal anatexis during the KC episode. The felsic magmas would be linked to the Red granites, from the partial crustal melting, constituting the lighter and magnetic (but barely remanent) contribution (Supplementary Data Table 1). The synchronicity of these events has been suggested by the presence of a magmatic events, active at 1.38 Ga along the margins of the Congo Craton (Mäkitie et al., 2014; Blanchard et al., 2017). The ages obtained in the Victoria Lake (NE Congo Craton), tentatively fit those obtained in the KC as well as the orientation of their magnetic vectors. They present positive anomalies from + 50 to + 120 mGal, where a 5 km-thick sill-like body at middle to lower crust levels (21 – 26 km) is produced by a 1.38 Ga mantle plume. The modelling supports high density (3100 – 3400 kg/m^3), high susceptibility (0.08 S.I.) and a remanence component with intensity 11 A/m (Blanchard et al., 2017). Given the large uncertainty in both the Kunene paleomagnetic pole and the modelling of the Lake Victoria 1.38 Ga Kunene-Kibarian Complex, the comparison of the modelled remanence direction of lobes presents a broad similarity with the paleomagnetic pole for the same crustal block of Lake Victoria.

5.4. Evolution of KC in the Mesoproterozoic.

The magnetic map of SW Angola clearly shows a regional NE-SW crustal scale structure that separates the Archean to Paleoproterozoic Cassinga crust to the east from the Paleoproterozoic Eburnean crust to the west. Most of the magnetic lineaments depicted in the magnetic map are sharply cut and clipped by the KC boundaries, suggesting that this NE-SW structure (RBG and SZ) formed during Paleproterozoic times. Comparable scheme of extensive magmatism in the Kibarian event is detected in the Lake Victoria during the breakup of the Columbia/Nuna supercontinent (Pisarevsky et al., 2014) with portions of the Congo Craton (Tack et al., 2010) linked to intra-plate magmatism in zones of lithospheric thinning.

On the other hand, the southern KC bodies (Zebra Mountains and the Uanguembela Lobe) as well as the Paleoproterozoic Epupa basement to the south of the KC show magnetic lineaments

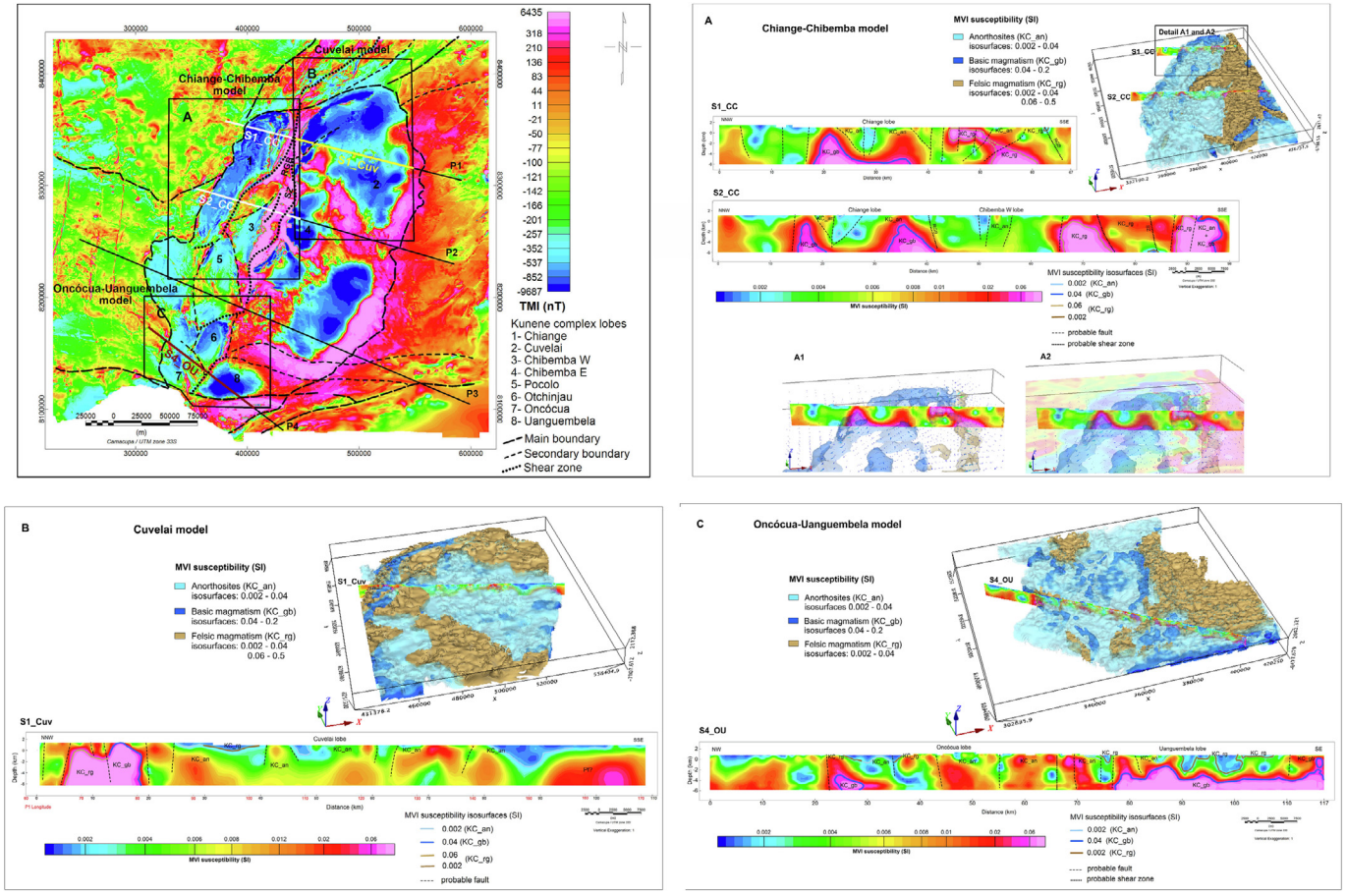

Fig. 7. Total magnetic intensity (TMI) map and location of 2.5D modelled profiles (P1, P2, P3 and P4) and 3D voxel models and sections (S1_CC, S2_CC, S1_Cuv and S4_OU). For each model are presented the MVI susceptibility isosurfaces representing the geological units that form KC and MVI susceptibility sections extracted from the amplitude of magnetization voxels. Interpreted geological units: KC_an – anorthosites, KC_gb – gabbros and KC_rg – Red granites. (A) Chiange-Chibemba MVI susceptibility model and extracted sections (S1_CC and S2_CC). In detail is presented the S1_CC section and MVI susceptibility isosurfaces of 0.04 (mafic) and 0.06 (felsic) with magnetization vectors distribution (A1) and information presented on A1 with overlap of the TMI grid (A2). (B) Cuvelai MVI susceptibility model and S1_Cuv section. (C) Oncócua-Uanguembela MVI susceptibility model and S4_OU section. (For interpretation of the references to colour in this figure legend, the reader is referred to the web version of this article.)

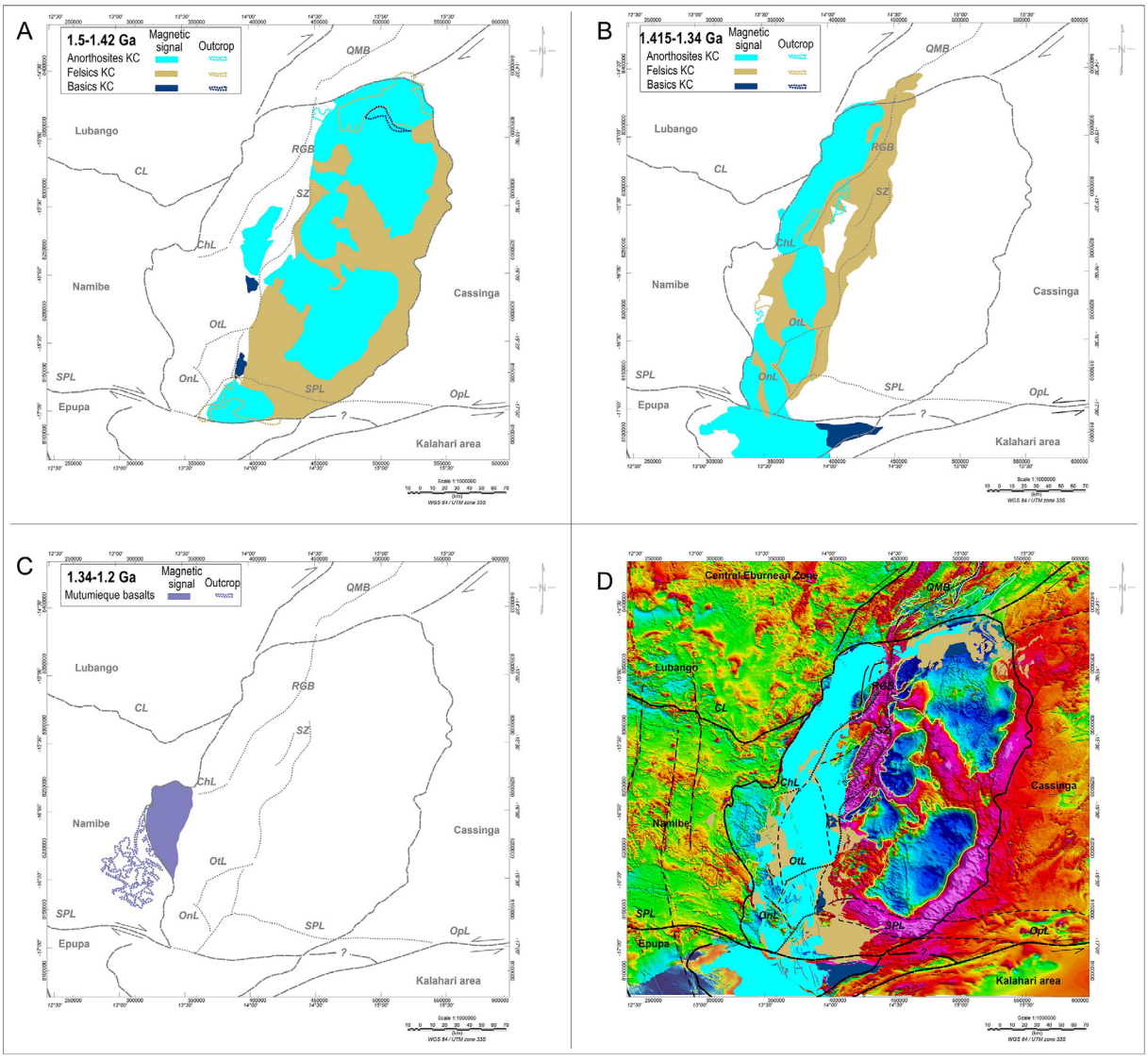

Fig. 8. Chronological evolution of the Kunene Complex. (A) Extensive anorthositic magmas and granites of the eastern KC (1.5–1.42 Ga) in NE-SW orientation, with no evidences of deformation in transtensional stages. The Uanguembela Lobe, located further south, presents an E-W disposition likely related to a complex system of shears affecting the crust in NNE-SSW and E-W directions. (B) The magmas emplaced to the W of the KC show distorted and narrow magnetic signals with more lineaments. It is still in a collisional context dominated by transpressive shearing processes with a change in the subduction angle, towards higher convergence velocity. Zebra Mountains and the lobes to the W of the KC (Chiange and Oncócua) are emplaced between 1390 Ma and 1370 Ma (even up to 1340 Ma). (C) Pull apart or negative flower system probably developed, leading the erosion of the KC lobes, the deposition of the Ompupa basin and subsequent emplacement of the Mutumieque basalts. Again, a variation from transpressional to a distensional context is evidenced by the subsequent deposition of sedimentary sequences and intrusion of a large number of alkaline to toleiitic dykes between 1320 Ma and 1100 Ma. This last extensional context probably signals the end of the subduction of the Kibarian belt, promoting the breakup of the Nuna supercontinent. (D) Present day outcrops of the KC units with the TMI map as background. It is highlighted the remanent bodies of the KC, major structures and structural domains.

ENE-WSW oriented (Figs. 2 and 8). This structure NE-SW is suggested as the continuation of the Mesoproterozoic Kibaran Belt from the Democratic Republic of Congo beneath the Kalahari cover (Fernandez-Alonso et al., 2012). The magnetic lineaments and NW-dipping crustal disturbances are shown by Euler solutions (Fig. 5). This suggests a complex strike-slip system responsible for crustal thrusting and the generation of distinct macro-scale structures. The ENE-WSW-trending Mesozoic Opuwo Lineament (OpL, Fig. 8) may mark an ancient suture and possible subduction zone found between the Cassinga crust, clearly older and thick, and a crust where the Kalahari area is involved to the south. This would agree with the subvertical structures modelled in Profile 3 (Fig. 6C). Given the existence of Paleoproterozoic cortical planes of weakness (Quipungo Mobile Belt, QMB), the magmas accumulate in these regions, fractioning and generating anorthositic melts. In turn, granitic magmas are generated by cortical thermal processes. The contrast in density and viscosity between the anorthositic magmas with respect to the partially molten bedrock and the granitic melts favors the ascent of the anorthositic melts. The relatively high viscosity and low density of the anorthositic magmas, favored diapiric ascent rather than lateral magma flow (Maier et al., 2013). Fractional crystallization of underplated mantle-derived melts at lower crustal levels is commonly suggested for generating large masses of anorthosite magmas (p.e., Ashwal, 1993). Regarding the Kunene Complex, some authors argued for a dominant extensional context favored by the deep ascent of an undefined mantle-plume (e.g., Mayer et al, 2004; Drüppel et al., 2007; Maier et al., 2013). Nevertheless, Lehmann et al. (2020, 2023) described top-to-the-W and top-to-the-NE shearing structures both in the Mesoproterozoic anorthosite and Red granites and in the Paleoproterozoic wall

rocks, which lead them to suggest that the KC emplacement was related to a contractional regime.

The events leading to the formation of the KC show a clear temporal progression (Fig. 8). First the parental melts of the Humpata basalts (Paleoproterozoic mafic igneous rocks W of the KC in Fig. 1) would generate the melts in NW Namibia. The enrichement in MgO, Cr and Ni, as well as O, Nd and S isotope characteristics of KC suggest primary magmas maily mantle-derived basatls (Maier et al., 2013). They likely intruded the first anorthositic melts of the Angolan KC (1530–1500 Ma) in an extension-dominated context within the regional compression (Fig. 9A). Subsequently, the large volume of anorthositic magmas and granites of the eastern KC (1500–1420 Ma) and some granites to the NW of Namibia were emplaced (Figs. 8A and 9B). The anorthositic suites represent mantle-derived magmas ponded at Moho depths which anorthositic massifs were formed by rising of feldspathic fluids with density and viscosity favored diapiric ascent of the anorthositic melts. The associated granitoids cropping out surrounding the KC lobes were derived from blending of mantle-derived material with Paleoproterozoic crustal material. The heat supplied from mantle-derived magma would cause crustal anatexis, forming the granitoid magmas. Potential hydrothermal activity would be derived from the intrusion of the Red granites as evidenced by mineral manetic content. The magnetic anomalies to the E of the KC, smoother and more homogeneous than those in the W, as well as absence of deformation of the lineaments, suggest that there were no dominant compressional structures or internal deformation in the KC. It may suggest that the emplacement was associated with transtensional stages. This arrangement would be explained with crustal fracturing and uplift processes (induced by subduction of low angle or low rate) since the prolongation of the magnetic lineaments coincides with a set of gravimetric and magnetic Euler solutions (Fig. 9B). At this stage, a contrast is already seen in the disposition of the so-called Uanguembela Lobe, with respect to the rest of the KC. This may indicate a complex system of shears affecting the crust in the NNE-SSW and E-W directions, as evidenced by magnetic mapping and sigmoidal lineaments in western lobes, which induce the geometry of the lobes.

Between 1390 Ma and 1370 Ma, the setting previously described seems to change slightly. The anorthositic and granitic magmas emplaced in the W of the KC occupy a minor lateral extent, showing distorted magnetic signals and more lineaments are observed (Fig. 8B). Subsequentely, the absence of deformation of NW-SE structures (Fig. 3) leads us to interpreting them in terms of post-KC to post-Mesoproterozoic and report the transition from a compressive to an extensional scenario. The collisional setting continues, but by emplacing narrow KC lobes and deflected magnetic lineations in the W, indicating a change in the subduction angle (Opuwo lineament), towards higher convergence velocity (Fig. 9C). Between 1390 Ma and 1370 Ma (even up to 1340 Ma), which is the age of emplacement of the Zebra Mountains and the lobes to the W of the KC (Chiange and Oncócua lobes), the fundamentally transtensional context changes to a context dominated by transpressive shearing processes. To the W-SW of the KC, a pull apart or negative flower system probably develops, which directly influences the erosion of the KC lobes and the deposition of the large Ompupa basin, which are subsequently intruded by basic phyllonian magmas as Mutumieque basalts (Fig. 8C). The change from a clearly transpressional to an extensional context is evidenced by the subsequent deposition of sedimentary sequences (Mesoproterozoic metasedimentary rocks in Fig. 1) and intrusion of a large number of alkaline to tholeiitic dykes between 1320 Ma and 1100 Ma. This last extensional context probably signals the end the Kibarian Belt. In any case, the lack of

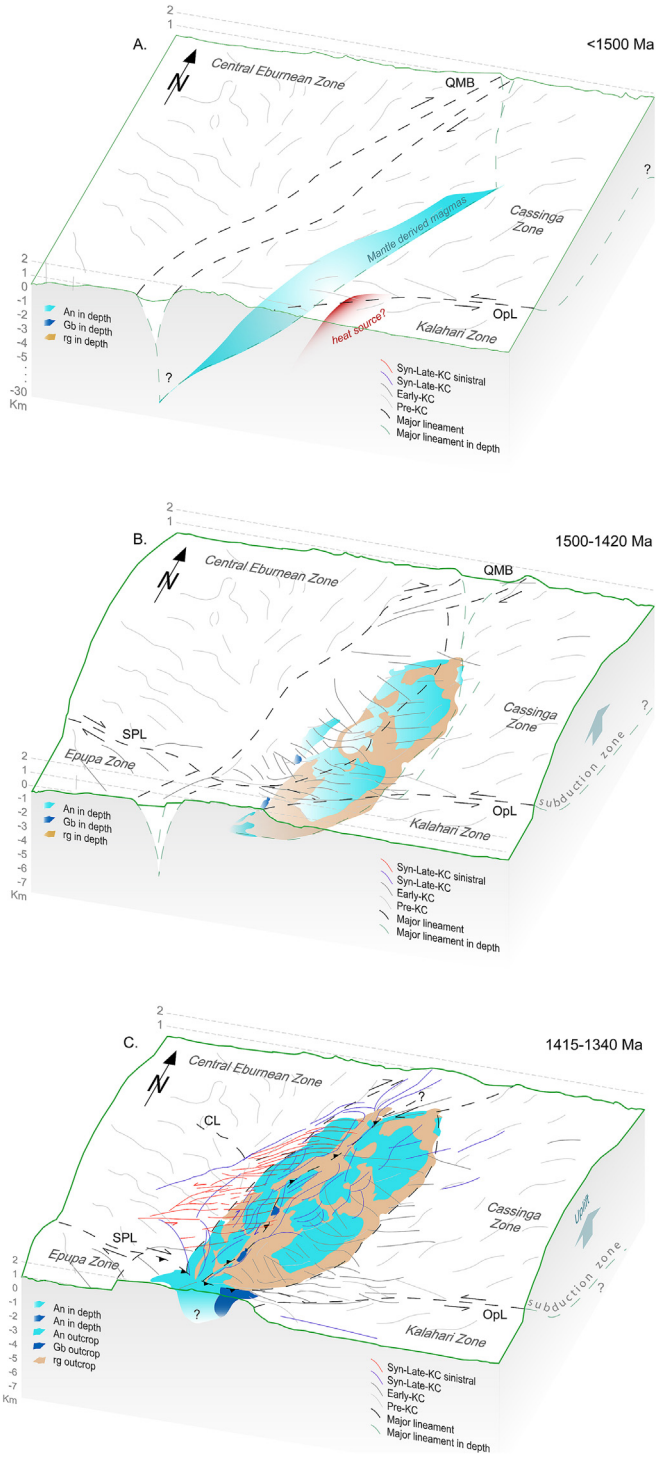

Fig. 9. Block diagram if three satges of KC development. (A) Mantle accumulation (anorthositic suites from mantle-derived magmas ponded at Moho depths) between 1.54–1.5 Ga and early anorthosite pulses in favor of the precursor Quipungo Mobile Belt (QMB). The major subduction lineament is located Opuwo Lineament (OpL), likely corresponding to the Kibarian Belt continuation, presents a parallel trend to the Early-KC structures formed in this or next stage. (B) Emplacement of the eastern mafic bodies and granites in a stage of great lateral extension in a transtensional context. Development of the Opuwo Lineament (OpL) with a low angle or low rate leading uplift processes. (C) Migration of the mantle system westwards with deformation in a complex contractional setting with shearing structures involving western KC mafic rocks and granite-related melt generation. Significant tectonic uplift in a continue collisional context, with a change in the subduction angle or towards higher convergence velocity.

deformation of these dykes and later dykes (1.1 Ga norites, Fig. 8D) indicates the absence of collisional processes and marks the transition from a compressional to an extensional scenario, promoting the breakup of the Nuna supercontinent.

5.5. Economic relevance

The massive anorthosite of KC noteworthy comprises ores of Ti, V, P and REE (Villanova-de-Benavent et al., 2017), whereas geochemical works point out the possible enrichment of MgO, Cr and Ni in NW Namibia (Maier et al., 2013), suggesting a high potential to host Ni-Cu-rich sulfides. Furthermore, satellite intrusions of the Zebra Mountains reported Ni–Cu–PGE sulfide mineralization (Haldar, 2017). This work therefore allows to possibly increase the economic interest of the KC as a possible source of important minerals. This is especially reflected in resources of magnetite, ilmenite and hematite-ilmenite (Ti-Fe) (Milesi et al., 2006). Thanks to this work, it is possible to discern rocks mainly carrying magnetite (anorthosite or gabbros of KC) or hematite-bearing rocks in presence of the ubiquitous magnetite (Red granites of KC). High positive magnetic anomalies linked to the E boundary of the KC could be produced by hydrothermal activity derived from the intrusion of the Red granites. Possible non-redox reaction, from magnetite to hematite (Otake et al., 2007; Zhao et al., 2019; Xing et al., 2021), may have been the main mechanism for the transformations of iron oxides in nature, especially in hydrothermal environments.

According to recently acquired ambient noise seismic data and available drill-holes in the study area (Carvalho et al., 2024), the lobes of the KC hidden beneath the Kalahari Basin are placed at depths shallower than 200 m, thus increasing the potential of the KC as a mineral resource. The KC rocks are rich in magnetite and titanium minerals, as products of segregation of the basic magma occurring in alignments that underline tectonics, often in a NNE-SSW direction (Santos, 1969). In this NNE-SSW to NE-SW longitudinal strip, Fe and Ti mineralizations occur, outcropping in KC, concentrated in main magnetic lineaments, as the south of the RGB, and especially the part that separates the lobes of Chiange and Pocolo. Other concentrations of mineralizations have been detected in the remanent bodies of anorthosites, significantly the north of Chiange and Poloco lobes and in the southernmost gabbroic body, south of the Uanguembela lobe (Araújo and Guimarães, 1992). Minerals in KC are mainly Ti-magnetite and to a lesser extent ilmenite, as well as aluminous spinel, apatite, olivine or graphite in cumulates corresponding to exsolutions where the minerals are concentrated (Villanova-de-Benavent et al., 2017). These studies confirm the previously known economic potential in Fe-Ti and also V, P and REE. The anorthosites analyzed by Gleißner et al. (2010) revealed contents of plagioclase, pyroxene, amphibole, apatite, olivine, ilmenite and magnetite, with apatite (Ce, Pr, Nd, Sm, Gd) and high REE values in white anorthosites. Regarding dark anorthosites, they present high Nb and V concentrations contained in ilmenite. In this work, the content of single domain (SD) magnetite is proven in the mafic terms of the KC, what can contain from 0.2% to 1% of V, potentially turning the KC into a main source of vanadium.

Considering the sharp boundary of the magnetic anomalies produced by the mafic bodies of the KC, confirmed by the magnetic modelling, it is expected that these mafic bodies are placed at shallow depths below the Kalahari Formation. According to magnetic modelling of profile P1 (see Fig. 6), the Kalahari Formation would present a shallowing from 85 km to 88 km (< 100 m). For profile P2 (Fig. 6) the Kalahari cover presents the thinnest areas: (i) From 100 km to 105 km with 35 m thick (passive seismic) and <50 m (magnetic), (ii) Between 168 km to 180 km a shallowing is suggested up to 88 m thick (passive seismic) and ~70 m (magnetic data). For profile P3, between 205 km and 249 km (Kalahari thickness <100 m). Recent geoelectrical and time domain electromagnetic modelling also confirmed these thicknesses for the Kalahari cover (Ramalho et al., 2023; Francés et al., 2024). Therefore, the modelling suggests that large areas with relatively good logistics conditions and where gabbroic/anorthositic shallow bodies could be further explored, helping defining areas of economic interest under the Kalahari cover.

6. Conclusions

(1) Magnetic data of excellent quality are available from the PLANAGEO Project. This allowed us to determine tectonic setting for the KC during the Mesoproterozoic times.

(2) Petrophysical analysis reveals contrasting magnetic properties in the main units of the KC: Anorthosites present medium susceptibility (0.0040 S.I.), high remanence (7.6518 A/m) and relative high density (2749 kg/m^3); gabbros display medium–high magnetic susceptibility (0.0150 S.I.), very high remanence (29.3330 A/m) and density (2810 kg/m^3); Red granites present the highest susceptibility (0.0272 S.I), very low remanence (0.0999 A/m) and low density (2644 kg/m^3). Isothermal Remanent Magnetization analyses show that mafic units (basement and KC) mainly contain magnetite, whereas felsic units present low and high coercive minerals. The exceptional remanence recorded in the mafic KC in contrast with very high susceptibility of contouring Red granites served as main constraint to model 2.5D sections and 3D inversions.

(3) Magnetic mapping helped to define the shape of the 11 KC composing lobes of the KC. The outcropping lobes in Angola (N to S) are: Chiange, Otchinjau, Oncócua and Uanguembela, whose real extension of the latter three was not known so far. The Pocolo and the Chibemba W lobes have been isolated. All of them, except Chibemba W and Uanguembela lobes, would be part of the second stage of KC formation (~1.34 –1.415 Ga). The Zebra Mountains Lobe would form part of this second stage of intrusion (1363 – 1385 Ma, Ernst et al., 2014). Four other lobes are covered by the Kalahari Formation, from N to S: Cuvelai, Chibemba E, Queulo and Cahama, newly defined in this work. These covered lobes along with Chibemba W and Uanguembela lobes compose the early stage of intrusion (~1.42 – 1.49 Ga). They are of special relevance due to their economic potential under the Kalahari Formation (<100 m in some areas).

(4) The main boundaries identified in this work are the Quipungo Mobile Belt (QMB), suggested as the precursor suture of the KC and separator of the Central Eburnean and Cassinga domains. The Red Granite Belt (RGB) likely constitutes a shearing dislocated continuation of the QMB. The Shear Zone (SZ) splits E to W lobes, being an active shear during 1385 – 1370 Ma (Rodrigues et al., 2021). The E-W trending Cainde lineament (CL), deflected by KC, constitutes the limit between the Central Eburnean and Namibe zones. The Serpa Pinto Line (SPL) is a major ESE-WNW fault, along which the southern KC components and wall rocks are thrusted northwards, splitting the Angolan KC and Zebra Mountains lobes. The Opuwo Lineament (OpL), constitutes a major subduction lineament, likely corresponding to the Kibarian Belt continuation and splitting the Kalahari area from the Cassinga domain (Fig. 2).

(5) The wall rocks were generally constituted by Paloproterozoic igneous rocks, with Neoarchean metamorphic evidences in the E and sedimentary basin to the W, constituted by Paleo to Neoproterozoic metasedimentary rocks. Mantle-derived melts accumulated at the base of the crust would generate melts in NW Namibia, probably lead to the first anorthositic melts of the Angolan KC (1530 – 1500 Ma) in an extension-dominated context in a

regional compression. Anorthosites crystalized at different depths until emplacement at mid-crust levels, in successive mafic magmatism related to mantle upwellings with long-live magmas (≥100 Ma). The heat supplied from mantle-derived magma would cause crustal anatexis, forming the granitoid magmas and mixing of mantle-derived material. Large anorthositic magmas and non deformed bodies in the east KC (1500 – 1400 Ma) and granites associated were emplaced, evidencing no compressional structures in transtensional stages explained by low-angle subduction to the NW. NE-SW oriented lobes probably justify an emplacement in a transtensional context. At this age, the oblique E-W Uanguembela Lobe may indicate complicated shears derived from crustal displacements in the Kibarian Belt. Between 1390 Ma and 1370 Ma, age of Zebra Mountains and the western lobes of the KC, more lineaments with reduced extent are recorded in a transpressive shearing stage. To the W-SW of the KC, a pull apart or negative flower system probably developed, leading to erosion of the KC lobes and the deposition of the Ompupa basin, subsequently intruded by mafic magmas as Mutumieque basalts (1340 – 1200 Ma).

CRediT authorship contribution statement

T. Mochales: Writing – review & editing, Writing – original draft, Visualization, Software, Methodology, Formal analysis, Data curation, Conceptualization. **E. Merino-Martínez:** Writing – review & editing, Writing – original draft, Project administration, Methodology, Data curation, Conceptualization. **C. Rey-Moral:** Writing – review & editing, Writing – original draft, Software, Methodology, Conceptualization. **A. Machadinho:** Writing – review & editing, Writing – original draft, Visualization, Validation, Software. **J. Carvalho:** Writing – review & editing, Project administration, Methodology. **P. Represas:** Writing – review & editing, Visualization, Methodology. **J.L. García-Lobón:** Writing – review & editing, Supervision, Project administration, Funding acquisition, Conceptualization. **M.C. Feria:** Visualization. **R. Martín-Banda:** Writing – review & editing, Conceptualization. **M.T. López-Bahut:** Visualization. **D. Alves:** Visualization. **E. Ramalho:** Visualization. **J. Manuel:** Visualization, Project administration. **D. Cordeiro:** Visualization.

Declaration of competing interest

The authors declare that they have no known competing financial interests or personal relationships that could have appeared to influence the work reported in this paper.

Acknowledgments

This work is a result of the National Geological Plan of Angola (PLANAGEO) and Investigación de procesos geológicos y recursos mineros críticos para la transición energética en Angola y en España (PIE-PLANAGEO). This project was supported by the Government of the Republic of Angola and implemented by the Geological Survey of Angola (IGEO), under the oversight of the Angolan Ministry of Mineral Resources, Oil and Gas (MIREMPET). Further analytical data and isotopic results were also supported by the subsidiary programme "Ayudas Extraordinarias Menciones Excelencia Severo Ochoa" of the CN IGME-CSIC (project AECEX2021, grant 15903). We would like to express our gratitude for the assistance provided by the local staff during our fieldwork. We also highly appreciate the contribution of the staff of Impulso Industrial Alternativo to this project. The Geotransfer group (University of Zaragoza) and the staff of the Paleomagnetism laboratory (University Polytechnic of Burgos) kindly helped us with the laboratory analyses. Isabel Fanlo, Nacho Subias (University of Zaragoza), Mario Iglesias kindly provided samples of areas with complex access that were used in this work. Part of this work was performed by T. Mochales as a Visiting Fellow at the Institute for Rock Magnetism (IRM) by funding from the University of Minnesota and National Science Foundation (award NSF-EAR 2153786). A. Machadinho thanks the Portuguese Foundation for Science and Technology (FCT) support, Geosciences Center project UIDB/ 00073/2020 (doi:10.54499/UIDB/00073/2020), University of Coimbra and and GeoBioTec project UIDB/04035/2020 (doi:10.54499/UIDB/04035/2020), Nova School of Science and Technology. The authors are very grateful to Dr. Geissler and an anonymous reviewers for their suggestions to improve this paper.

Appendix A. Supplementary data

Supplementary data to this article can be found online at https://doi.org/10.1016/j.gsf.2025.102030.

References

Araújo, A.G., Guimarães, F., 1992. Geologia de Angola, Notícia explicativa da Carta Geológica à escala 1: 1 000 000. Serviço Geológico de Angola, Luanda (in Portuguese).

Ashwal, L.D., 1993. Anorthosites. Springer, Heidelberg.

Ashwal, L.D., Twist, D., 1994. The Kunene complex, Angola/Namibia: a composite massif-type anorthosite complex. Geol. Mag. 131 (5), 579–591. https://doi.org/10.1017/S0016756800012371.

Ashwal, L.D., Bybee, G.M., 2017. Crustal evolution and the temporality of anorthosites. Earth-Sci. Rev. 173, 307–330. https://doi.org/10.1016/j.earscirev.2017.09.002.

Balmino, G., Vales, N., Bonvalot, S., Briais, A., 2012. Spherical harmonic modelling to ultra-high degree of Bouguer and isostatic anomalies. J. Geodesy 86, 499–520. https://doi.org/10.1007/s00190-011-0533-4.

Baxe, O.S.S., 2007. Geocronologia de Complexos máfico-ultramáficos: exemplo sa série superior do complexo de Niquelândia, Brasil e do Complexo do Kunene, Angola. Unpublished Ph.D. Thesis, Universidade de Brasilia, Instituto de Geociências, 77 p. (in Portuguese).

Blanchard, J.A., Ernst, R.E., Samson, C., 2017. Gravity and magnetic modelling of layered maficultramafic intrusions in large igneous province plume centre regions; Case studies from the: 1.27 Ga Mackenzie, 1.38 Ga Kunene-Kibaran, 0.06 Ga Deccan and 0.13-0.08 Ga High Arctic events. Can. J. Earth Sci. 54, 290–310.

Bonvalot, S., Balmino, G., Briais, A., Kuhn, M., Peyrefitte, A., Vales N., Biancale, R., Gabalda, G., Reinquin, F. y Sarrailh, M., 2012. World Gravity Map. Commission for the Geological Map of the World. Eds. BGI-CGMW-CNES-IRD, Paris.

Brower, A.M., 2017. Understanding Magmatic Timescales and Magma Dynamics in Proterozoic Anorthosites: a Geochronological and Remote Sensing Investigation of the Kunene Complex (Angola). Unpublished PhD Dissertation, University of Witwatersrand, Johannesubrg, South Africa, 86 p.

Brandt, S., Will, T.M., Klemd, R., 2007. Ultrahigh-temperature metamorphism and anticlockwise PT paths of sapphirine-bearing orthopyroxene-sillimanite gneisses from the Proterozoic Epupa Complex, NW Namibia Precambr. Res 153 (3–4), 143–178. https://doi.org/10.1016/j.precamres.2006.11.016.

Brown, L.L., McEnroe, S.A., 2008. Magnetic properties of anorthosites: A forgotten source for planetary magnetic anomalies? Geophys. Res. Lett. 35, L02305.

Bybee, G.M., Hayes, B., Owen-Smith, T.M., Lehmann, J., Ashwal, L.D., Brower, A.M., Hill, C.M., Corfu, F., Manga, M., 2019. Proterozoic massif-type anorthosites as the archetypes of long-lived (≥100 Myr) magmatic systems—New evidence from the Kunene Anorthosite Complex (Angola). Precambrian Res. 332, 105393. https://doi.org/10.1016/j.precamres.2019.105393.

Campeny, M., Proenza, J.A., Castillo-Oliver, M., Torró, L., Villanova-de-Benavent, C., Melgarejo, J.C., Gonçalves, A.O., Román-Alpiste, M.J., Blanco-Quintero, I.F., Llovet, X., Farré-de-Pablo, J., 2023. Petrology, metallogeny and U-Pb geochronology of the Paleoproterozoic mafic-ultramafic Hamutenha intrusion, Angolan Shield. J. Afr. Earth Sci. 197, 104733. https://doi.org/10.1016/j.jafrearsci.2022.104733.

Carvalho, H., 1984. Estratigrafia do Précâmbrico de Angola. Garcia de Orta, Serie Geologia, Instituto Investigação Científica Tropical 7 (1-2), 1-66 (in Portuguese).

Carvalho, H., Alves, P., 1990. Gabbro-Anorthosite Complex of SW Angola/NW Namibia. Comunicações Instituto de Investigação Científica Tropical (Portugal), Série de Ciências da Terra, 2, Lisboa, pp. 5–64.

Carvalho, H., Alves, P., 1993. The Precambrian of SW Angola and NW Namibia: General Remarks, Correlation Analysis, Economic Geology. Comunicações Instituto de Investigação Científica Tropical (Portugal), Série de Ciências da Terra, 4, Lisboa, 38 p.

Carvalho, H., Tassinari, C.C., Alves, P.H., Guimarães, F., Simões, M., 2000. Geochronological review of the Precambrian in western Angola: links with Brazil. J. Afr. Earth Sci. 31 (2), 383–402. https://doi.org/10.1016/S0899-5362(00)00095-6.

Carvalho, J., Alves, D., Borges, J., Caldeira, B., Cordeiro, D., Machadinho, A., Oliveira, A., Ramalho, E., Rodrigues, J.F., Lorente, J.M., Ditutala, M., García-Lóbon, J.L., Máximo, J., Carvalho, C., Labaredas, J., Ibarra, P., Manuel, J., 2024. Depth estimation of pre-Kalahari basement in Southern Angola using seismic 1 noise measurements and drill-hole data. J. Appl. Geophys. 230, 105498. https://doi.org/10.1016/j.jappgeo.2024.105498.

Charlier, B., Namur, O., Bolle, O., Latypov, R., Duchesne, J.C., 2015. Fe–Ti–V–P ore deposits associated with Proterozoic massif-type anorthosites and related rocks. Earth-Sci. Rev. 141, 56–81. https://doi.org/10.1016/j.earscirev.2014.11.005.

Corner, B., Cartwright, J., Swart, R., 2002. Volcanic passive margin of Namibia: A potential fields perspective. Geological Society of America Special Paper 362, 203–220. https://doi.org/10.1130/0-8137-2362-0.203.

Delhal, J., Ledent, D., Cordani, U.G., 1969. Ages Pb/U, Sr/Rb et Ar/K de Formations Métamorphiques et Granitiques du Sud-Est du Brésil (États de Rio de Janeiro et Minas Gerais). Annales De La Société Géologique De Belgique 92, 271–283 (in French).

Delhal, J., Ledent, D., Torquato, J.R., 1976. Nouvelles données géochronologiques relatives au complexe gabbro-noritique et charnockitique du bouclier du Kasai et à son prolongement en Angola. Ann. Soc. Géol. Belg., 99, 211-226 (in French). https://popups.uliege.be/0037-9395/index.php?id=5361.

Delor, C., Lafon, J. M., Rossi, P., Cage, M., Pato, D., Chevrel, S. Lê Metour, J., Matukov, D., Sergeev, S., 2006. Unravelling Precambrian crustal growth of central west Angola: Neoarchaean to Siderian inheritance, main Orosirian accretion and discovery of the "Angolan" Pan African Belt. Em: Abstract of the 21st Colloquium of African Geology, Maputo, Mozambique, pp. 3-5.

Dobmeier, C., 2006. Emplacement of Proterozoic massiftype anorthosite during regional shortening: Evidence from the Bolangir anorthosite complex (Eastern Ghats Province, India). Int. J. Earth Sci. 95 (4), 543–555.

Drüppel, K., Littmann, S., Romer, R.L., Okrusch, M., 2007. Petrology and isotope geochemistry of the Mesoproterozoic anorthosite and related rocks of the Kunene Intrusive Complex, NW Namibia. Precambrian Res. 156, 1–31.

Duchesne, J.C., Liégeois, J.P., Vander Auwera, J., Longhi, J., 1999. The crustal tongue melting model and the origin of massive anorthosites. Terra Nova 11, 100–105.

Ellis, R.G., de Wet, B., MacLeod, I.N., 2012. Inversion of magnetic data for remanent and induced sources. ASEG Extended Abstracts 2012, 1–4.

Ernst, R.E., Pereira, E., Hamilton, M.A., Van-Dunem, M.V., Rodriques, J., Tassinari, C. C., Teixeira, W., 2014. Intraplate magmatic 'barcode' record of the Angola portion of the Congo craton: newly dated magmatic events at 1502 and 1109 Ma and implications for Nuna and Rodinia supercontinental reconstructions. Precambrian Res. 230, 103–118.

Escuder-Viruete, J., Gumiel, J.C., Merino-Martínez, E., Da Cruz Correia, J., Quintana, L., 2021. Carta Geológica de Angola à escala 1:250.000, Folhas Sul D-33/S e Sul D-32/Z, Namibe, e Notícia Explicativa. Ministério dos Recursos Minerais, Petróleo e Gás, UTE PLANAGEO (IGME-LNEG-Impulso) - Instituto Geológico de Angola (IGEO), Luanda (Angola), 188 p.

Fernandez-Alonso, M., Cutten, H., De Waele, B., Tack, L., Tahona, A., Baudet, D., Barritt, S.D., 2012. The Mesoproterozoic Karagwe-Ankole Belt (formerly the NE Kibara Belt): The result of prolonged extensional intracratonic basin development punctuated by two short-lived far-field compressional events. Precambrian Res. 216–219, 63–86.

Ferreira, E., Lehmann, J., Rodrigues, J.F., Hayes, B., Merino-Martínez, E., Milani, L., Bybee, G.M., Owen- Smith, T.M., García-Lobón, J.L., Tassinari, C.G., Ueckermann, H., Sato, K., Silva, P.B., Correia, J., Labaredas, J., Duarte, L., Molekwa, A.M., Manuel, J., da Mata, A., Victorino, L., 2024. Zircon U-Pb and Lu-Hf isotopes reveal the crustal evolution of the SW Angolan Shield (Congo Craton). Gondwana Res. 131, 317–342. https://doi.org/10.1016/j.gr.2024.03.010.

Francés, A.P., Ramalho, E.C., Monteiro Santos, F., Llorente, J.M., Mateus, T., Martin Banda, R., Cuervo, I., García Lobón, J.L., Dala, V., Ditutala, M., Famorosa, A., Victorino, A.M., 2024. Contribution of the time domain electromagnetic method to the study of the Kalahari transboundary multilayered aquifer systems in Southern Angola. Hydrogeol. J. 32, 1709–1727. https://doi.org/10.1007/s10040-024-02822-x.

Geosoft, 2013. Sharpening using Iterative Reweighting Inversion, Oasis. http://bit.ly/11NAzAn.

Gleißner, P., Drüppel, K., Taubald, H., 2010. Magmatic evolution of anorthosites of the Kunene Intrusive Complex, NW Namibia: Evidence from oxygen isotope data and trace element zoning. J. Petrol. 51, 897–919. https://doi.org/10.1093/petrology/egq005.

Goscombe, B., Foster, D.A., Gray, D., Wade, B., Marsellos, A., Titus, J., 2017. Deformation correlations, stress field switches and evolution of an orogenic intersection: The Pan-African Kaoko-Damara orogenic junction, Namibia. Geosci. Front. 8, 1187–1232. https://doi.org/10.1016/j.gsf.2017.05.001.

Goscombe, B., Gray, D., Armstrong, R., Foster, D.A., Vogl, J., 2005. Event geochronology of the Pan-African Kaoko Belt, Namibia. Precambrian Res. 140, 103.e1–103.e41. https://doi.org/10.1016/j.precamres.2005.07.003.

Haddon, I.G., 2005. The sub-Kalahari geology and tectonic evolution of the Kalahari basin, Southern Africa. University of the Witwatersrand, Johannesburg, pp. 24–34.

Haldar, S.K., 2017. Chapter 3. Deposits of Africa. In: Haldar, S.K. (Ed.), Platinum-Nickel-Chromium Deposits. Geology, Exploration and Reserve Base, Ed. Elsevier, pp. 63-96. https://doi.org/10.1016/C2014-0-00851-9.

Hanson, R.E., 2003. Proterozoic geochronology and tectonic evolution of southern Africa. Geol. Soc. London. Spec. Pub. 206, 427–463. https://doi.org/10.1144/GSL.SP.2003.206.01.20.

Jelsma, H., Perritt, S.-H., Armstrong, R.A., Ferreira, H.F., 2011. SHRIMP U–Pb zircon geochronology of basement Rocks of the Angolan Shield, western Angola. In: Proceedings of the 23rd CAG, Johannesburg. Council for Geoscience, pp. 395–409.

Jelsma, H.A., McCourt, S., Perritt, S.H., Armstrong, R.A., 2018. The Geology and Evolution of the Angolan Shield, Congo Craton. In: Siegesmund, S., Basei, M.A.S., Oyhantçabal, P., Oriolo, S. (Eds.), Geology of Southwest Gondwana, Regional Geology Reviews. Springer International Publishing, Cham, pp. 217–239. https://doi.org/10.1007/978-3-319-68920-3_9.

Korpershoek, H., 1970. Geology of the Cassinga north area; explanatory note of the 1/50,000 geological map. Companhia Mineira do Lobito (unpublished report).

Kröner, A., Rojas-Agramonte, Y., Wong, J., Wilde, S.A., 2015. Zircon reconnaissance dating of Proterozoic gneisses along the Kunene River of northwestern Namibia. Tectonophysics 662, 125–139. https://doi.org/10.1016/j.tecto.2015.04.020.

Kröner, A., Rojas-Agramonte, Y., 2017. Mesoproterozoic (Grenville-age) granitoids and supracrustal rocks in Kaokoland, northwestern Namibia. Precambrian Res. 298, 572–592. https://doi.org/10.1016/j.precamres.2017.07.008.

Labaredas, J., Correia, J., Rodrigues, J. F., 2021. Carta Geológica de Angola à escala 1:250.000, Folhas Sul E-33/A, Espinheira, e Notícia Explicativa. Ministério dos Recursos Minerais, Petróleo e Gás, UTE PLANAGEO (IGME-LNEG-Impulso) - Instituto Geológico de Angola (IGEO), Luanda (Angola), 158 p.

Larson, T.E., 2015. Mesoproterozoic Paleomagnetism of the Southern Congo Craton. Ph.D. thesis. Yale University, p. 80.

Laske, G., Masters, G., Ma, Z. and Pasyanos, M., 2013. Update on CRUST1.0 - A 1-degree Global Model of Earth's Crust, Geophys. Res. Abstracts, 15, Abstract EGU2013-2658, 2013.

Lehmann, J., Bybee, G.M., Hayes, B., Owen-Smith, T.M., Belyanin, G., 2020. Emplacement of the giant Kunene AMCG complex into a contractional ductile shear zone and implications for the Mesoproterozoic tectonic evolution of SW Angola. Int. J. Earth Sci. 109, 1463–1485. https://doi.org/10.1007/s00531-020-01837-5.

Lehmann, J., Brower, A.M., Owen-Smith, T.M., Bybee, G.M., Hayes, B., 2023. Landsat 8 and Alos DEM geological mapping reveals the architecture of the giant Mesoproterozoic Kunene Complex anorthosite suite (Angola/Namibia). Geosci. Fronti. 14, 101620. https://doi.org/10.1016/j.gsf.2023.101620.

Li, H., Li, L., Zhang, Z., Santosh, M., Liu, M., Cui, Y., Yang, X., Chen, J., Yao, T., 2014. Alteration of the Damiao anorthosite complex in the northern North China Craton: implications for high-grade iron mineralization. Ore Geol. Rev. 57, 574–588.

Lowrie, W., 1997. Fundamentals of Geophysics. Cambridge University Press, Cambridge, UK, p. 354.

Macleod, I.N., Ellis, R.G., 2013. Magnetic Vector Inversion, a Simple Approach to the Challenge of Varying Direction of Rock Magnetization. Australian Society of Exploration Geophysicists, Extended Abstracts, Melbourne, 2013, pp. 1-4.

Maier, W.D., Rasmussen, B., Fletcher, I.R., Li, C., Barnes, S.-J., Huhma, H., 2013. The Kunene anorthosite complex, Namibia, and its satellite intrusions: geochemistry, geochronology, and economic potential. Econ. Geol. 108, 953–986.

Mäkitie, H., Data, G., Isabirye, E., Mänttäri, I., Huhma, H., Klausen, M.B., Pakkanen, L., Virransalo, P., 2014. Petrology, geochronology and emplacement model of the giant 1.37 Ga arcuate Lake Victoria Dyke Swarm on the margin of a large igneous profince in eastern Africa. J. Afr. Earth Sci. 97, 273–296. https://doi.org/10.1016/j.jafrearsci.2014.04.034.

Matmon, A., Hidy, A.J., Vainer, S., Crouvi, O., Fink, D., Erel, Y., Team, A., Arnold, M., Aumaître, G., Bourlès, D., Keddadouche, K., Horwitz, L.K., Chazan, M., 2015. New chronology for the southern Kalahari Group sediments with implications for sediment-cycle dynamics and early hominin occupation. Quat. Res. 84, 118–132. https://doi.org/10.1016/j.yqres.2015.04.009.

Maxbauer, D.P., Feinberg, J.M., Fox, D.L., 2016. MAX UnMix: A web application for unmixing magnetic coercivity distributions. Comput. Geosci. 95, 140–145. https://doi.org/10.1016/j.cageo.2016.07.009.

Mayer, A., Hofmann, A.W., Sinigoi, S., Morais, E., 2004. Mesoproterozoic Sm–Nd and U–Pb ages for the Kunene Anorthosite Complex of SW Angola. Precambrian Res. 133, 187–206. https://doi.org/10.1016/j.precamres.2004.04.003.

McCourt, S., Armstrong, R.A., Jelsma, H., Mapeo, R.B.M., 2013. New U–Pb SHRIMP ages from the Lubango region, SW Angola: insights into the Palaeoproterozoic evolution of the Angolan Shield, southern Congo Craton, Africa. J. Geol. Soc. 170, 353–363. https://doi.org/10.1144/jgs2012-059.

Merino-Martínez, E., Rodrigues, J.F., Ferreira, E., Chamizo, M., Potti, J., Labaredas, J., Francés, A., Morais, A. Oliveira, A., E. Pereira, E., 2022. Mapa Geológico de Angola à escala 1:1.000.000, e Notícia Explicativa. Zona UTE (Região Sul de Angola). Ministério dos Recursos Minerais, Petróleo e Gás, UTE PLANAGEO (IGME-LNEG-Impulso) - Instituto Geológico de Angola (IGEO), Luanda (Angola), 105 p.

Merino-Martínez, E., Goicoechea, P.P., 2022. Mapa e Notícia Explicativa da Carta Geológica de Lubango, Folha SUL D-33/N, escala 1: 250.000. Instituto Geológico de Angola. Ministério dos Recursos Minerais, Petróleo e Gas, Luanda (Angola), 244 p.

Milani, L., Lehmann, J., Bybee, G.M., Hayes, B., Owen-Smith, T.M., Oosthuizen, L., Delport, P.W.J., Ueckermann, H., 2022. Geochemical and geochronological constraints on the Mesoproterozoic Red Granite Suite, Kunene AMCG Complex of Angola and Namibia. Precambrian Res. 379, 106821. https://doi.org/10.1016/j.precamres.2022.106821.

Milesi, J.P., Toteu, S.F., Deschamps, Y., Feybesse, J.L., Lerouge, C., Cocherie, A., Penaye, J., Tchameni, R., Moloto-A-Kenguemba, G., Kampunzu, H.A.B., Nicol, N., Duguey, E., Leistel, J.M., Saint-Martin, M., Ralay, F., Heinry, C., Bouchot, V., Doumnang Mbaigane, J.C., Kanda Kula, V., Chene, F., Monthel, J., Boutin, P., Cailteux, J., 2006. An overview of the geology and major ore deposits of Central Africa: explanatory note for the 1:4,000,000 map "Geology and major ore deposits of Central Africa". J. Afr. Earth Sc. 44 (4–5), 571–595.

Merino-Martínez, E. Ferreira, E., Valverde-Vaquero, P., Rodrigues, J.F., Escuder-Viruete, J., García-Lobón, J.L., Beranoaguirre, A., Feria, M.C., Rey-Moral, C., Silva, P.B., González-Cuadra, P., Sousa, J.C., Potti, J., Máximo, J., Gutiérrez-Medina, M., Gumiel, J.C., Galán, G., Mochales, T., Manuel, J., Cordeiro, D., Tassinari, C., Montero, P., Sato, k., Fuenlabrada, J.M., Galindo, C., 2024. U-Pb ages in the southern Angolan Shield and implications for the evolution of the Kunene Complex during the Mesoproterozoic. Geotemas 20, 1349.

Morais, I., Batista, M. J., Represas, P., Albardeiro, L., Prazeres, C., Plastov, J. M., Sousa, J. C., Bravo, P., Sousa, P., Carvalho, J., Rodrigues, J. F., Oliveira, D., and Cordeiro, D., 2023. Metallogenetic potencial of the Paleoproterozoic mafic-ultramafic Hamutenha intrusion (SW Angola). New data from PLANAGEO project, EGU General Assembly 2023, Vienna, Austria, 23–28 Apr 2023, EGU23-15202. https://doi.org/10.5194/egusphere-egu23-15202, 2023.

Nafe, J.E., Drake, C.L., 1957. Variation with depth in shallow and deep water marine sediments of porosity, density and the velocities of compressional and shear waves. Geophysics 22, 523–552.

Otake, T., Wesolowski, D.J., Anovitz, L.M., Allard, L.F., Ohmoto, H., 2007. Experimental evidence for non-redox transformations between magnetite and hematite under H2-rich hydrothermal conditions. Earth Planet. Sci. Lett. 257 (1–2), 60–70. https://doi.org/10.1016/j.epsl.2007.02.022.

Pereira, E., Tassinari, C.G., Rodrigues, J.F., Van-Dúnen, V., 2011. New data on the deposition age of the volcano-sedimentary Chela Group and its Eburnean basement: implications to post- Eburnean crustal evolution of the SW of Angola. Comunicações Geológicas Do LNEG 98, 29–40.

Pereira, E., Rodrigues, J.F., Tassinari, C., Van-Dúnen, M.V., 2013. Geologia da região de Lubango, SW de Angola. Evolução no contexto do cratão do Congo. Laboratório Nacional de Energia e Geologia, (LNEG), Portugal. Instituto Geológico de Angola, IGEO, 164 p.

Piper, J.D.A., 1974. Magnetic properties of the Cunene Anorthosite Complex, Angola. Phys. Earth Planet. Inter. 9 (4), 353–363. https://doi.org/10.1016/0031-9201(74)90063-6.

Pisarevsky, S., Elming, S.A., Pesonen, L., Li, Z.X., 2014. Mesoproterozoic paleogeography: Supercontinent and beyond. Precambrian Res. 244, 207–225. https://doi.org/10.1016/j.precamres.2013.05.014.

Ramalho, E.C., Francés, A.P., Monteiro Santos, F., da Mata, A.V., 2023. 3D electrical structure definition of aquifer systems in the Kalahari basin in Southern Angola based on legacy data reprocessing. J. Appl. Geophys. 211, 104968. https://doi.org/10.1016/j.jappgeo.2023.104968.

Rey-Moral, C., Mochales, T., Merino-Martínez, E., García Lobón, J.L., López Bahut, M. T., Martín-Banda, R., Feria, M.C., Ballesteros, D., Machadinho, A., Alves, D., 2022. Recording the largest anorthositic complex worldwide: The Kunene Complex (KC), SW Angola. Precambrian Res. 379, 106790. https://doi.org/10.1016/j.precamres.2022.106790.

Robertson, D.J., France, D.E., 1994. Discrimination of remanence-carrying minerals in mixtures, using isothermal remanent magnetization acquisition curves. Phys. Earth Planet. Int. 82, 223–234.

Rodrigues, J. F., Merino-Martínez, E., Ferreira, E., 2021. Mapa Tectónico de Angola à escala 1:1.100.000, e Notícia Explicativa. Ministério dos Recursos Minerais, Petróleo e Gás, UTE PLANAGEO (IGME-LNEG-Impulso) - Instituto Geológico de Angola (IGEO), Luanda (Angola), 101 p.

Salminen, J., Hanson, R., Evans, D.A.D., Gong, Z., Larson, T., Walker, O., Gumsley, A., Söderlund, U., Ernst, R., 2018. Direct Mesoproterozoic connection of the Congo and Kalahari cratons in proto-Africa: Strange attractors across supercontinental cycles. Geology 46, 1011–1014. https://doi.org/10.1130/G45294.1.

Santos, L., 1969. Ocorrências de ilmenites no Sul de Angola. Bol. Serviços De Geologia e Minas De Angola 20, 8–21 (in Portuguese).

Seth, B., Armstrong, R.A., Brandt, S., Villa, I.M., Kramers, J.D., 2003. Mesoproterozoic U–Pb and Pb–Pb ages of granulites in NW Namibia: reconstructing a complete orogenic cycle. Precambrian Res. 126, 147–168. https://doi.org/10.1016/S0301-9268(03)00193-1.

Seth, B., Armstrong, R.A., Büttner, A., Villa, I.M., 2005. Time constraints for Mesoproterozoic upper amphibolite facies metamorphism in NW Namibia: a multi-isotopic approach. Earth Planet. Sci. Lett. 230, 355–378. https://doi.org/10.1016/j.epsl.2004.11.022.

Silva, A.F., 2005. A Geologia da República de Angola desde o Paleoarcaico ao Paleozóico Inferior. Instituto Nacional de Engenharia, Tecnologia e Inovação, IP. 44 p. (in Portuguese).

Silva, A.T.F., Torquato, J.R., Kawashita, K., 1973. Alguns dados geocronológicos pelo método K/Ar da região de Vila Paiva Couceiro, Quilengues e Chicomba (Angola). Serviço De Geol. e Minas De Angola 24, 29–46 (in Portuguese).

Silva, P.B., Oliveira, A., Duarte, L., Labaredas, J., Goicoechea, P., 2021. Carta Geológica de Angola à escala 1:250.000, Folha Sul D-33/T, Chibia, e Notícia Explicativa. Ministério dos Recursos Minerais, Petróleo e Gás, UTE PLANAGEO (IGME-LNEG-Impulso) - Instituto Geológico de Angola (IGEO), Luanda (Angola), 255 p. (in Portuguese).

Simón, S.J., Wei, C., Ellmies, R., Yang, H., Soh Tamehe, L., 2017. New SIMS U-Pb age on zircon from the Epembe carbonatite dyke, NW Namibia: Implications for Mesoproterozoic evolution of carbonatites at the southern margin of the Congo Craton. J. Afr. Earth Sci. 135, 108–114. https://doi.org/10.1016/j.jafrearsci.2017.08.011.

Tack, L., Wingate, M.T.D., De Waele, B., Meert, J., Belousova, E., Griffin, B., Tahon, A., Fernandez-Alonso, M., 2010. The 1375 Ma Kibaran event in Central Africa: prominent emplacement of bimodal magmatism under extensional regime. Precambr. Res. 180, 63–84. https://doi.org/10.1016/j.precamres.2010.02.022.

Tegtmeyer, A., Kröner, A., 1985. U–Pb zircon ages for granitoid gneisses in northern Namibia and their significance for Proterozoic crustal evolution of southwestern Africa. Precambrian Res. 28 (3–4), 311–326. https://doi.org/10.1016/0301-9268(85)90036-1.

Thompson, D.T., 1982. EULDPH: A new technique for making computer-assisted depth estimates from magnetic data. Geophysics 47, 31–37. https://doi.org/10.1190/1.1441278.

Torquato, J.R., 1977. Geotectonic outline of Angola. Cahiers O.R.S.T.O.M., Sér. Géol., vol. IX, num. 1/2, 15–34.

Vermaak, C.F., 1981. Kunene Anorthosite Complex. In: Hunter, D.R. (Eds.), Precambrian of the Southern Hemisphere. Developments in Precambrian Geology, 2, Elsevier, Amsterdam, pp. 578–599.

Villanova-de-Benavent, C., Torró, L., Castillo-Oliver, M., Campeny, M., Melgarejo, J.C., Llovet, X., Galí, S., Gonçalves, A.O., 2017. Fe–Ti (–V) oxide deposits of the kunene anorthosite complex (SW Angola): Mineralogy and Thermo-Oxybarometry. Minerals 7 (12), 246. https://doi.org/10.3390/min7120246, 27 pp.

Xing, Y., Brugger, J., Etschmann, B., Tomkins, A.G., Frierdich, A.J., Fang, X., 2021. Trace element catalyses mineral replacement reactions and facilitates ore formation. Nat Commun. 12 (1), 1388. https://doi.org/10.1038/s41467-021-21684-5.

Zhao, Y., De Vries, J., van den Berg, A., Jacobs, M., van Westrenen, W., 2019. The participation of ilmenite-bearing cumulates in lunar mantle overturn. Earth Planet. Sci. Lett. 511, 1–11.